

N 7 1 - 2 3 9 8 3

N 69-23700

NASA CR-72779

## FINAL TECHNICAL REPORT

# RESEARCH INTO THE FEASIBILITY OF THIN-METAL AND OXIDE-FILM CAPACITORS

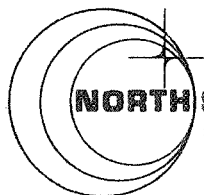
CASE FILE  
COPY

by  
G. V. Jorgenson  
and  
W. H. Graves

March 1971



Prepared Under Contract No. NAS 12-551 by



**NORTH STAR** RESEARCH AND DEVELOPMENT INSTITUTE  
3100 THIRTY-EIGHTH AVENUE SOUTH • MINNEAPOLIS, MINNESOTA 55406

Lewis Research Center  
NATIONAL AERONAUTICS AND SPACE ADMINISTRATION

Distribution of this report is provided in the interest of information exchange and should not be construed as endorsement by NASA of the material presented. Responsibility for the contents resides with the organization that prepared it.

"Requests for copies of this report should be referred to:

NASA Scientific and Technical Information Facility  
P.O. Box 33, College Park, Maryland 20740"

N 69-23700

NASA CR-72779

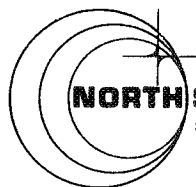
**FINAL TECHNICAL REPORT**

**RESEARCH INTO THE  
FEASIBILITY OF THIN-METAL  
AND OXIDE-FILM CAPACITORS**

by  
G. V. Jorgenson  
and  
W. H. Graves

March 1971

Prepared Under Contract No. NAS 12-551 by



**NORTH STAR** RESEARCH AND DEVELOPMENT INSTITUTE  
3100 THIRTY-EIGHTH AVENUE SOUTH • MINNEAPOLIS, MINNESOTA 55408

Lewis Research Center  
NATIONAL AERONAUTICS AND SPACE ADMINISTRATION  
Cleveland, Ohio

Dr. Francisc C. Schwarz, Technical Monitor



## TABLE OF CONTENTS

	<u>Page</u>
SUMMARY . . . . .	1
INTRODUCTION. . . . .	3
EXPERIMENTAL WORK . . . . .	6
Equipment . . . . .	6
Deposition Parameters . . . . .	17
Capacitor Tests . . . . .	25
CONCLUSIONS AND RECOMMENDATIONS . . . . .	48
REFERENCES. . . . .	50
APPENDIX	
NEW TECHNOLOGY APPENDIX	



## LIST OF FIGURES

<u>Number</u>	<u>Title</u>	<u>Page</u>
1	Sputtering System for Thin Film Capacitor Development . . .	7
2	Vacuum System for Evaporation of Aluminum Capacitor Electrodes. . . . .	8
3	Schematic of Mask- and Target-Changer Mechanism for Multi-Layer Capacitor Fabrication . . . . .	10
4	Partially Assembled Mask- and Target-Changer. . . . .	11
5	Detailed View of Mask Changing Disk . . . . .	12
6	Sloan DTM-3 Deposit Thickness Monitor . . . . .	14
7	Electrical Arrangement of the Sloan DTM-3 Deposit Thickness Monitor . . . . .	16
8	Laboratory Facility for Multiple Life-Testing of Thin Film Capacitors . . . . .	18
9	Multiple-Capacitor Life Test Unit . . . . .	19
10	Comparison of Sputtered Aluminum Films. . . . .	21
11	Experimental Capacitor Arrangements . . . . .	23
12	Equivalent Electrical Circuit of a Capacitor. . . . .	27
13	The Effect of Frequency on Dissipation Factor at 22°C for a Typical Double-Layer Silica Capacitor . . . . .	30
14	The Effect of Frequency on Dissipation Factor at 22°C for Two 6-Layer Silica-Aluminum Capacitors. . . . .	31
15	The Effect of Frequency on Capacitance at 22°C for Two 6-Layer Silica-Aluminum Capacitors. . . . .	32
16	The Effect of Frequency on Capacitance at Several Temperatures from -79 to 225°C for Silica-Aluminum Capacitor XIV . . . . .	34
17	The Effect of Frequency on Dissipation Factor at Three Temperatures for Silica-Aluminum Capacitor XIV. . . .	35
18	The Effect of Frequency on Dissipation Factor at Three Temperatures for Silica-Aluminum Capacitor XIV. . . .	36

# LIST OF FIGURES (Continued)

<u>Number</u>	<u>Title</u>	<u>Page</u>
19	The Effect of Frequency and Temperature on Capacitance of an Alumina-Aluminum Capacitor. . . . .	37
20	The Effect of Frequency and Temperature on Dissipation Factor of an Alumina-Aluminum Capacitor . . . . .	38
21	The Effect of 312 Hours Exposure to 150°C in Air on the Frequency-Capacitance Relationship. . . . .	40
22	The Effect of 312 Hours Exposure to 150°C in Air on the Frequency-Dissipation Factor Relationship . . . . .	41
23	Mean Values of the Dissipation Factor for Silica-Aluminum Capacitors as a Function of Electrode Thickness at 1.0 and 100 kHz. . . . .	42
24	Dissipation Factor as a Function of Frequency and Current . . . . .	44
25	The Effect of Long-Duration, High-Temperature Exposure on a Silica-Aluminum Capacitor at Four Frequencies. . . . .	45
26	The Effect of 1000 Hours Exposure of a Double-Layer Silica-Aluminum Capacitor to 250°C in Air . . . . .	46

RESEARCH INTO THE FEASIBILITY  
OF THIN METAL- AND OXIDE-FILM CAPACITORS

by

G.V. Jorgenson  
and  
W.H. Graves

NORTH STAR RESEARCH AND DEVELOPMENT INSTITUTE  
Minneapolis, Minnesota

March 1971

SUMMARY

This report covers a three-year program in which low energy radio frequency (rf) sputtering was utilized in an investigation of the feasibility of producing thin metal- and oxide-film capacitors. The objectives were to establish a useful configuration for a planar film filter capacitor consisting of densely packed parallel interconnected layers. The capacitors must have stable electrical properties and must be able to withstand high temperature environments. The original concept called for capacitors of one-half cubic centimeter of deposited material; that was later changed to 1.0  $\mu$ f capacitors. The requirement for the dielectric films is 2000 to 4000 Å thick.

Dielectric material systems examined in the development work included silica, alumina, titania, and lead zirconate titanate. Silica gave the best results, even with its lower dielectric constant, because it could be deposited at a higher rate and had more stable characteristics than the other materials. The majority of test capacitors were prepared with silica dielectrics and aluminum electrodes. Many alumina-aluminum capacitors were also tested, but they had lower thermal stability than the silica capacitors.

The silica-aluminum capacitors were made by rf sputter-depositing aluminum electrodes and silica dielectrics in an ultrahigh-vacuum system. Most were single- or double-layer (one or two dielectric layers) capacitors, with some having up to ten dielectric layers. They have very good temperature

stability from -79 to 250°C, and continue to function well at 500°C, but with larger temperature coefficients of capacitance and larger dissipation factors. Following an air bake at 250°C, the capacitance varies only 0.6 percent from 25 to 250°C. The highest capacitance density that has been achieved for these capacitors is 320  $\mu\text{f}$  per cubic centimeter of deposited material. The dissipation factor of the test capacitors was low, generally in the  $10^{-4}$  range at low frequency and in the mid  $10^{-2}$  range at high frequency.

The preferred electrode thickness was established as 1200 to 1500 Å, based on measurements of dissipation factor versus electrode thickness. Dielectric strength of the silica films is generally between  $2 \times 10^6$  and  $5 \times 10^6$  volts per centimeter. At  $2 \times 10^6$  volts per centimeter, the breakdown strength is 20 volts per 1000 Å of dielectric. Based on these measurements, and on the desire to keep thickness down to obtain high capacitance density, dielectrics were normally made 3000 Å thick. This would yield a capacitor with a working voltage of 25 volts with an adequate safety factor.

A mask and target changer was designed and fabricated for installation in the sputtering system. This mechanism will allow the alternate deposition of silica dielectric and aluminum electrodes without breaking vacuum. This system should make it possible to fabricate capacitors with more layers because less handling of the substrate will mean less chance for defects. However, time on the current program did not permit the changer to be evaluated for making multilayer capacitors.

It is recommended that, in a follow-on program, the maximum number of layers that can be stacked reliably using the mask and target changer be established, and the quality and yield of capacitors be determined. The techniques that are employed in making these multilayer high-temperature capacitors can then be engineered into a production process, and the full benefit of the research program can be obtained.

## INTRODUCTION

The National Aeronautics and Space Administration has a requirement for capacitors with capabilities beyond those now available. High capacitance per unit volume and low power dissipation are needed. Because the capacitors do not have to handle high power, their breakdown strengths can be relatively low. However, they must be very stable in high-temperature environments such as might be encountered on space flights near the sun, or in applications near nuclear reactors. North Star Research and Development Institute undertook a three-year program to develop a filter capacitor that would meet these requirements. More specifically, the properties needed were densely packed parallel interconnected layers producing a capacitor of 1.0  $\mu\text{f}$  capacitance. The capacitors must be able to tolerate high temperatures (up to 500°C). It was necessary to establish the electrical parameters such as capacitance and dissipation factor as functions of temperature and frequency in the ranges of -55° to 300°C and up to 100 kHz.

Several dielectric materials (titania, alumina, silica, lead zirconate titanate) and electrode materials (nickel, aluminum, titanium, copper) were screened during the early part of the program. The best combinations were established as alumina-aluminum and silica-aluminum. Of these, the highest degree of thermal stability was found in capacitors consisting of silica dielectrics and aluminum electrodes.

The bulk dielectric constant for silica is 3.75, and that for the sputter-deposited thin films is slightly less (usually about 3.2 to 3.6). For a material of any given dielectric constant, the capacitance per unit volume of a single-layer capacitor can be increased by decreasing the thickness of the deposited films, dielectric, and electrodes. The thinner layers give lower mass for a given number of layers, and a thinner dielectric gives increased capacitance. The limit to which the thickness of the dielectric can be decreased depends on the voltage that the capacitor must hold without breaking down. If the voltage requirements are very low (less than approximately 25 volts) thickness becomes limited by problems in manufacturing. As the dielectric

becomes very thin, an increasing percentage of the capacitors have shorts, and the yield decreases. This usually occurs at dielectric thicknesses below 2000 angstroms. The limit to which the electrode thickness can be decreased is governed by the conductivity of the electrode material. The sheet resistance of the electrodes must be kept very low to have capacitors with low dissipation factors.

Low-energy rf sputtering was used for the deposition of all dielectric films in this program. The aluminum electrodes were vacuum evaporated at first, and later they were also sputter deposited. The principal advantage of rf sputtering the bulk dielectric material for capacitor dielectrics rather than anodizing (Ref. 1), vacuum evaporating (Ref. 2), or reactively sputtering (Ref. 3), is the capability of depositing a film of the same stoichiometry as the target material. RF sputtering also produces films of high density with good adhesion and relatively free from pinholes.

Teflon dielectric capacitors provide an example of currently available capacitors with good temperature and electrical characteristics. They are operable to approximately 200°C and have low dissipation factor ( $2 \times 10^{-4}$  at 25°C). They also have relatively high capacitance density ( $0.01 \mu\text{f cm}^{-3}$  for the completed package). Ceramic capacitors have the highest capacitance densities except for electrolytic capacitors which are inferior in all other respects. Typical values for ceramic capacitors are  $0.25 \mu\text{f cm}^{-3}$ . The silica-aluminum capacitors that were developed in this program had excellent temperature stability to approximately 275°C and were operable at the highest test temperature (500°C). Dissipation factors of these capacitors were generally in the  $10^{-4}$  range at low frequency and in the mid  $10^{-2}$  range at high frequency. The capacitance density of the silica-aluminum capacitors was approximately  $300 \mu\text{f cm}^{-3}$  of deposited material. In a packaged capacitor consisting of a multilayer deposit on both surfaces of a very thin substrate, a capacitance density of  $10 \mu\text{f cm}^{-3}$  could probably be achieved. In the high capacitance sizes, the density could be made somewhat greater by putting several substrates in the same package.

The capacitor characteristics discussed above, *i.e.*, high density films with good adhesion, high temperature stability and capability, low dissipation factor, and high capacitance density, contribute to the overall high reliability that is required by NASA for long-duration space flights in hostile environments.

## EXPERIMENTAL WORK

Capacitors were fabricated by rf sputter deposition of thin dielectric layers and evaporation or rf sputter deposition of thin conducting electrodes on thin glass substrates. Early in the program the rf sputtering was moved from an oil pumped vacuum system to an ultrahigh vacuum system in a clean room to assure a contamination- and dust-free environment. Layers were stacked, and the electrodes were interconnected to give a parallel array of capacitors for high energy storage capacity per unit of substrate area. The capacitors were tested for capacitance and dissipation factor as functions of frequency and temperature, for dielectric strength as a function of dielectric thickness, and for dissipation factor as a function of electrode thickness. The capacitors were also subjected to long-term life tests at elevated temperatures.

### Equipment

Vacuum Systems. -- Three vacuum systems were employed for the production of test capacitors during the program. All dielectric films were rf sputtered, in an oil-diffusion-pumped system at first, and later in a Ultek 18-inch ultrahigh-vacuum system. The Ultek system was fitted with a 6-inch-high glass cylinder and a stainless steel plate with a center hole through which the sputtering target projected. This system is shown in North Star's Class 100 clean room in Figure 1. Pumping is by cryosorption for roughing and by titanium sublimation and ion pumping for high vacuum. No oil pumping is used, so no hydrocarbons can enter and become trapped in deposited films. Also, the ultrahigh-vacuum system, because of the very low pressures obtainable, has less background gas that can be incorporated in the films than does an oil-pumped system. This is important because some of the atoms of background gases are active, and over a period of time, they will react with atoms that make up the desired film and change the capacitor characteristics.

During the early stages of the investigation, the aluminum electrodes were vacuum evaporated in the oil-diffusion-pumped vacuum system shown in Figure 2. Later, the electrodes were sputter deposited in the same Ultek ultrahigh-vacuum system that was used for deposition of the silica dielectric.



FIGURE 1. SPUTTERING SYSTEM FOR THIN FILM CAPACITOR DEVELOPMENT

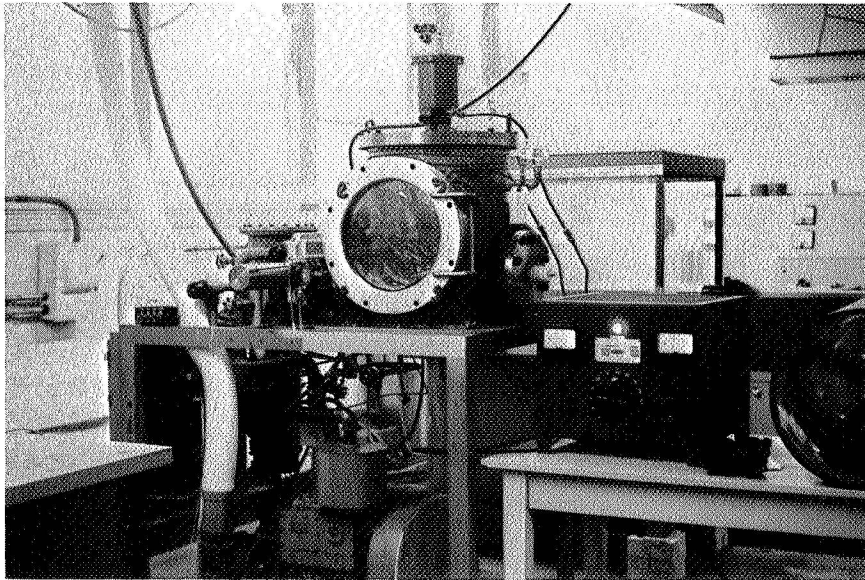


FIGURE 2. VACUUM SYSTEM FOR EVAPORATION OF ALUMINUM CAPACITOR ELECTRODES

Sputtering Module. -- All the sputtering was done with an R.D. Mathis Model SP 310 sputtering module. It consists of a 13.56 MHz 1.0 kw transmitter and a tuning unit. The transmitter is designed to feed a 50-ohm load, so the function of the tuning unit is to make the load 50 ohms for maximum coupling of power into the target. The tuning unit is supplied with two sizes of inductors to handle a range of target sizes from one to six inches diameter. Even though 5-inch-diameter targets were used, they carried more current when a magnetic field was used to increase plasma density than would normally be carried by a 6-inch-diameter target. A third size inductor had to be made so the high current load could be matched to the transmitter.

Mask and Target Changer. -- A mask and target changer system was fabricated. It was designed to allow the deposition of alternate layers of electrode and dielectric material without having to break the vacuum. Operation without breaking vacuum is necessary for multilayer capacitors to obtain high yields and to reduce the time required for pump-downs. A schematic diagram of the system is shown in Figure 3. The section labeled "A" operates the mask changer, and the section labeled "B" (also connected to a rotary feedthrough) changes targets. The aluminum target is mounted directly on the rf electrode for aluminum deposition. For silica deposition, a flat plate of silica is moved into place completely covering the aluminum target and very close to it. Figure 4 shows the partially assembled mask and target changer. The long parallel rails at the top carry the silica target into position for dielectric sputtering and out of the way for electrode sputtering. A disk carrying the masks can be seen below the rails, and the large disk is the main support for the entire assembly. At the bottom are two shafts that connect to rotary feedthroughs for doing the changing. Figure 5 gives a more detailed view of the mask-changing disk. The system is designed for taking four 3/4-inch square substrates. The three sets of masks are for odd-numbered electrodes, dielectric, and even-numbered electrodes. The hole in the center of each set of masks exposes the film thickness monitor to the depositing film. The large round hole allows the substrates to be loaded and the completed capacitors to be unloaded. The lid for that hole provides a close-fitting shutter to protect against dust particles falling on the samples during pump-down or during target changing. The triangular shaped piece at the left of the disk is a device for locking the disk in its various positions.

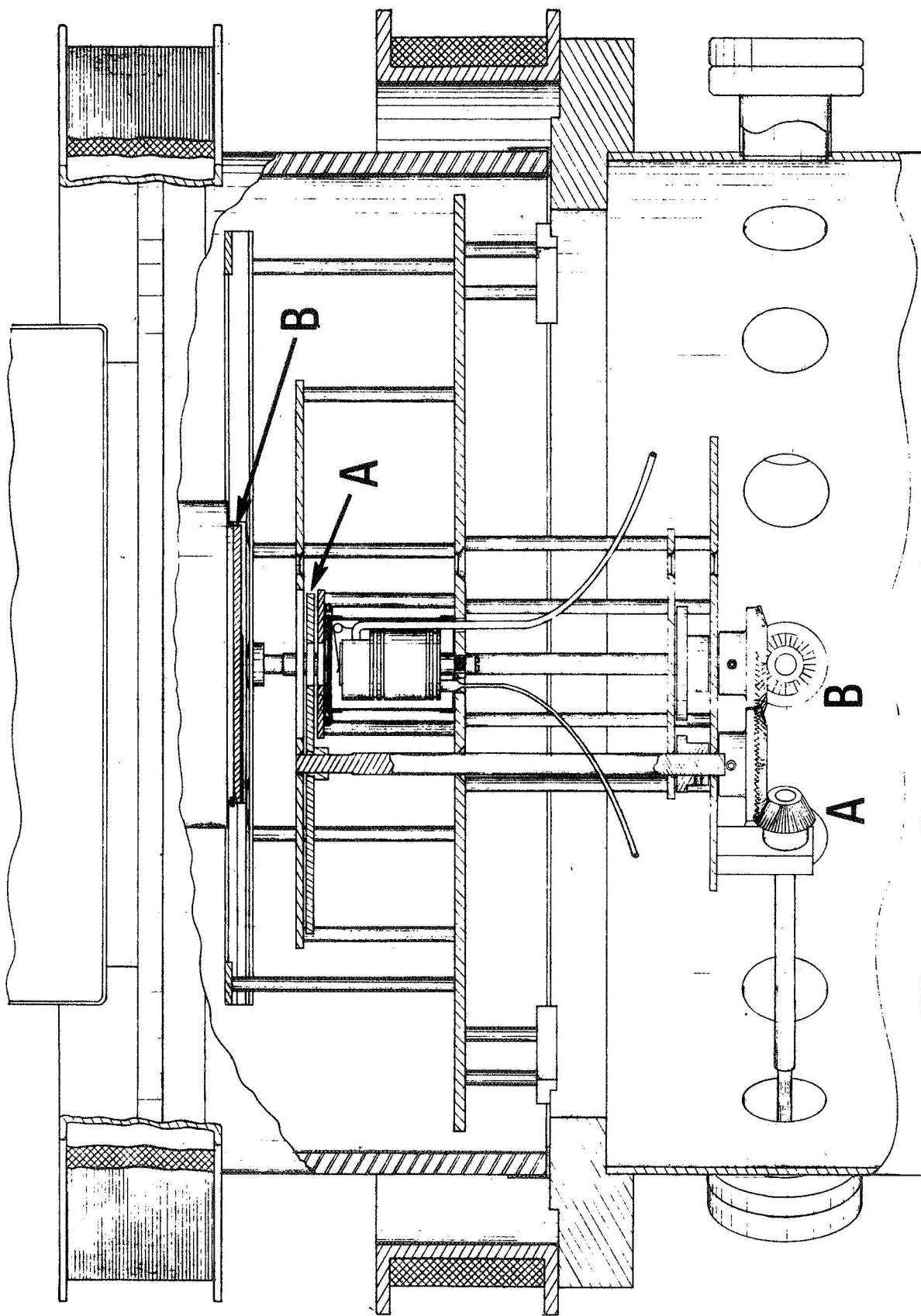


FIGURE 3. SCHEMATIC OF MASK- AND TARGET-CHANGER MECHANISM FOR MULTI-LAYER CAPACITOR FABRICATION

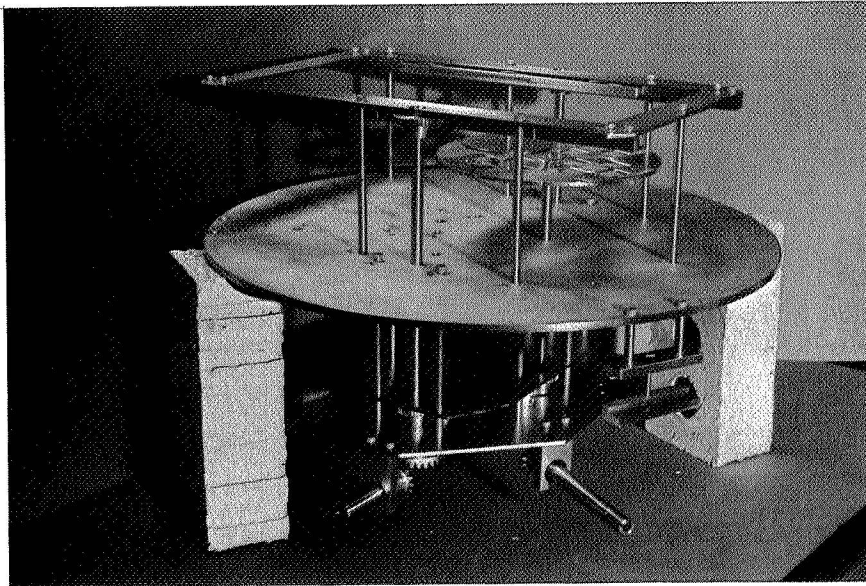


FIGURE 4, PARTIALLY ASSEMBLED MASK- AND TARGET-CHANGER

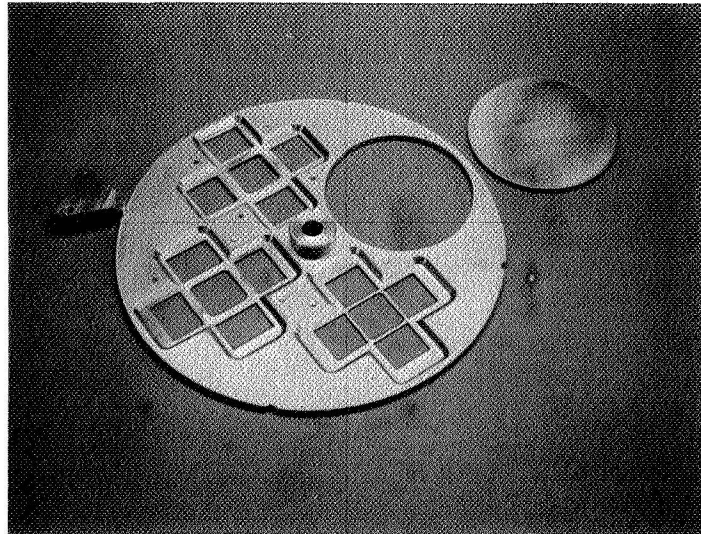


FIGURE 5. DETAILED VIEW OF MASK CHANGING DISK

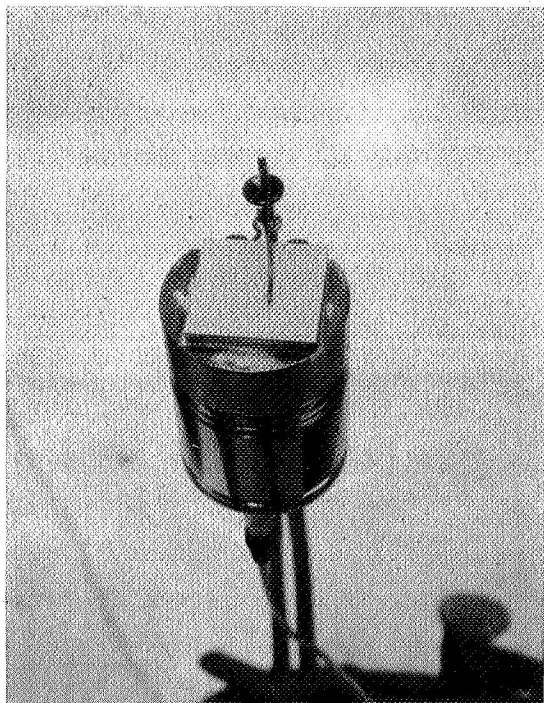
The specially shaped silica movable target that was required could not be obtained from General Electric Company because of their extended labor strike. An alternative supplier, West Coast Optical Company, was not able to fabricate the target successfully in time for use in the current contract, so the mask and target changer has not been fully tested.

Deposit Thickness Monitor. -- A deposit thickness monitor (Sloan Technology Corporation, Model DTM-3) was acquired for incorporation into the system. The monitor control and detection unit are pictured in Figure 6. The principal components are a 5 MHz quartz crystal (the sensing element) and a variable frequency oscillator. The variable frequency oscillator is tuned to the frequency of the quartz crystal and, as material deposits on the crystal, its oscillation frequency changes. The resultant beat frequency is calibrated to deposited film thickness.

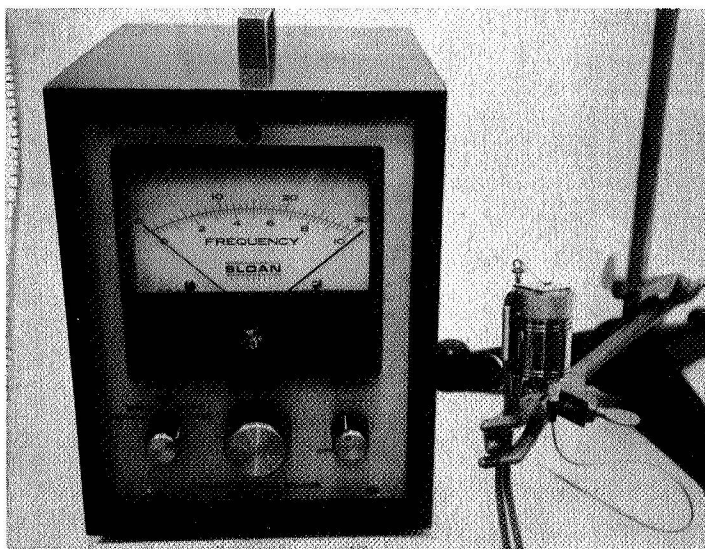
There are a number of problems inherent in operating the 5 MHz device in the hostile environment of a 13.56 MHz rf plasma. The crystal and the electric leads between it and the feedthrough act as antennas, picking up the 13.56 MHz signal and transmitting it back to the monitor control.

The accuracy of the monitor is also affected by an accumulation of charge from the plasma on the quartz crystal. The charge is usually negative because the electrons have higher mobility than do the ions. However, once the crystal becomes biased negatively with respect to the plasma, ions also bombard its surface.

The accuracy of the deposit thickness monitor is also affected by large temperature excursions of the quartz crystal. The crystal rests on a water-cooled copper block, but quartz has such a low thermal conductivity that the front surface can get hot by radiation from the plasma or from the hot target, or by electron bombardment. The latter becomes very important in the case where the monitor is mounted directly opposite the sputtering target. Secondary electrons are always ejected from a surface undergoing ion bombardment. Since the charge of the secondary electrons is opposite that of the ions, bombardment of the target by 1000 eV ions will cause the secondary electrons to be accelerated to 1000 eV away from the target. The direction



Sensing Element with Crystal Positioned



Monitor Control and Detection Unit

FIGURE 6. SLOAN DTM-3 DEPOSIT THICKNESS MONITOR

of travel of the electrons is perpendicular to a flat target surface. The magnetic field (axis perpendicular to target surface) that is applied to increase the plasma density condenses these electrons so that more arrive per unit area at the monitor crystal than leave per unit area of the target. These electrons add considerably to the thermal input of the crystal by giving up their kinetic energy on impact. They also give up their charge, biasing the crystal negatively. This causes ion bombardment, and the kinetic energy given up by the ions results in further heating of the crystal.

Several modifications were made to the thickness monitor to eliminate or substantially reduce these unwanted effects. Electrically, the modifications are shown in Figure 7. The crystal is separated from its oscillator, the latter being placed in the monitor cabinet. A 13.56 MHz filter was placed in the line between the crystal and the oscillator, and all leads were shielded and grounded. Also, the entire inside surface of the monitor case was covered with electromagnetic radiation shielding material. In the vacuum system, two metal meshes approximately 1.0 centimeter apart were mounted in front of the crystal and were grounded. That nearest to the crystal was approximately 0.5 centimeter from it. These meshes prevented penetration of the plasma to the surface of the crystal, thereby eliminating those charging effects. They also reduced the secondary electron bombardment and the thermal radiation. Some sensitivity was surrendered to accomplish this, because the meshes also reduce the amount of sputtered material arriving at the crystal.

The axis of the magnetic field was changed so that the secondary electrons would be deflected away from the monitoring crystal. This improved the operation of the crystal detector but changed the film thickness profile on the substrate. It appears that a magnetic field could be used successfully by utilizing several magnets arranged around the vacuum chamber. Power could be supplied alternately to different pairs of magnets in a cyclic manner during a sputtering run to cancel out nonuniformities in thickness profile.

The extensive modifications to the deposit thickness monitor have greatly increased its usefulness. Its operation is still not entirely

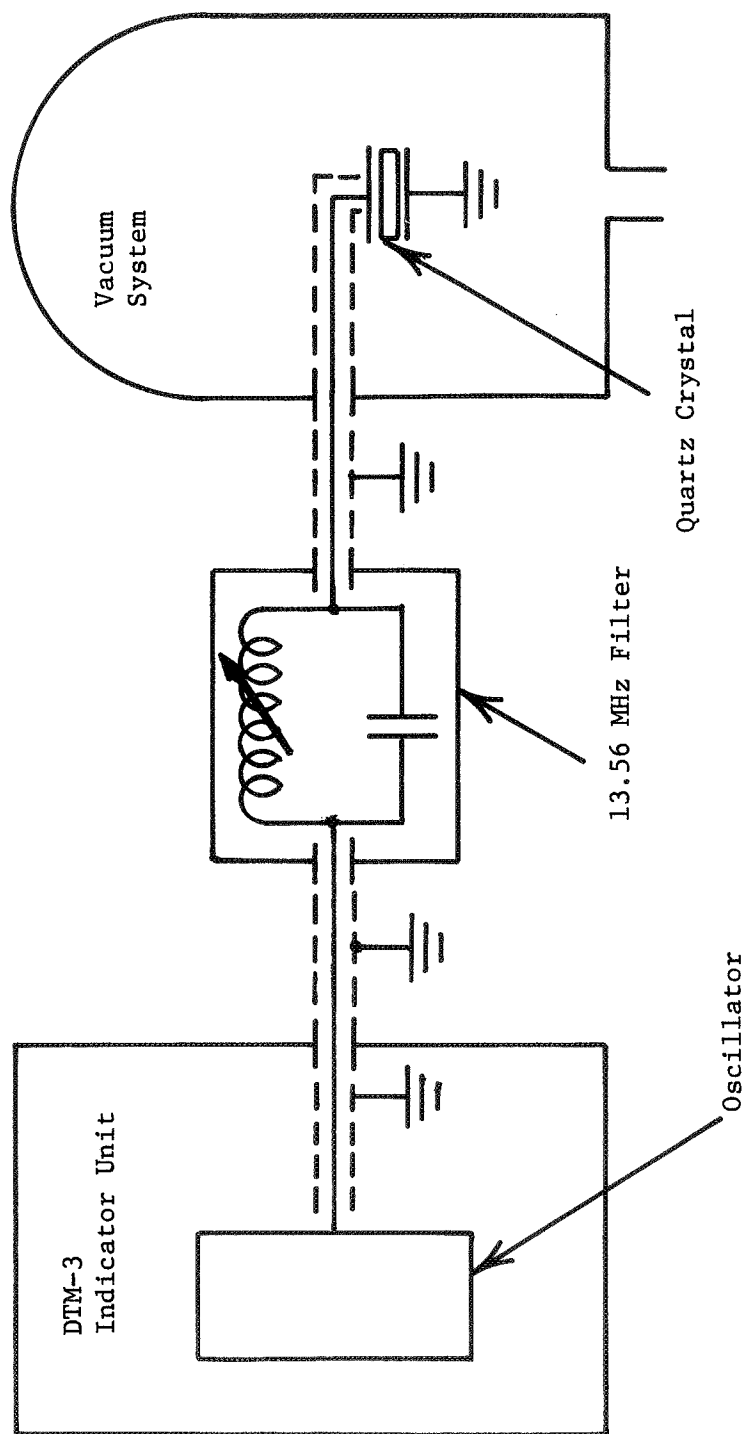


FIGURE 7. ELECTRICAL ARRANGEMENT OF THE SLOAN DTM-3 DEPOSIT THICKNESS MONITOR

satisfactory, but it can be used with a good degree of reliability. It was completely useless before the modifications were made.

Capacitor Test Setup. -- All capacitor tests at room temperature or higher temperatures were conducted in a forced horizontal air-flow oven (Despatch Oven Company Model LAD 1-42H). This oven has a temperature capability of 343°C. A one-inch-diameter ceramic tube was installed through a side wall to carry electric wires to the test capacitors. A multiposition switch that can maintain an applied voltage on all test capacitors, and remove the voltage from any one capacitor, connecting it to the test circuit, was mounted just outside the feedthrough. The applied voltage is 24.5 volts, rms, 60 Hz. The test circuit consists of a General Radio Type 1615A capacitance bridge and an audio generator. This instrumentation is capable of measuring capacitance and dissipation factor at frequencies from 200 Hz to 100 kHz. The setup is pictured in Figure 8. Figure 9 shows a capacitor test block that was fabricated for use in the oven. This test block can hold five of the 2.5 cm-by-2.5 cm capacitors. Those parts that are subject to thermal oxidation are nickel-plated, and the contacts are made from a corrosion-resistant spring brass. The contacts are mounted on ceramic standoffs.

Low-temperature electrical tests were run by encapsulating the test capacitor in a silicone elastomer (General Electric Company RTV 630). This encapsulation prevented erroneous readings caused by conductivity through moisture condensed on the surface of the capacitor. The encapsulated capacitor was cooled by dry ice.

#### Deposition Parameters

Silica. -- All the silica films were deposited from a 12.7 cm-diameter, 0.32 cm-thick disk of fused quartz (General Electric Company Type 101). The distance from the silica target to the substrate was approximately 3.8 cm for nearly all the sputtering runs.

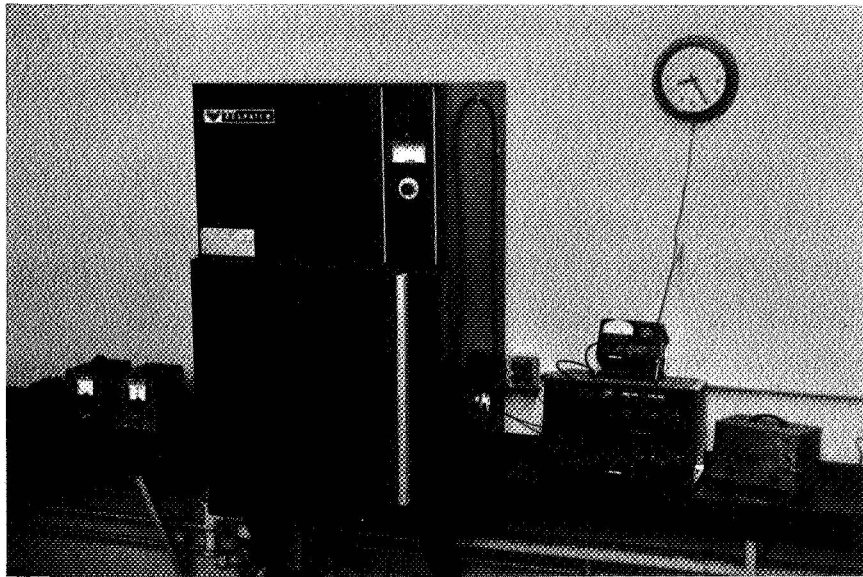


FIGURE 8. LABORATORY FACILITY FOR MULTIPLE  
LIFE-TESTING OF THIN FILM CAPACITORS

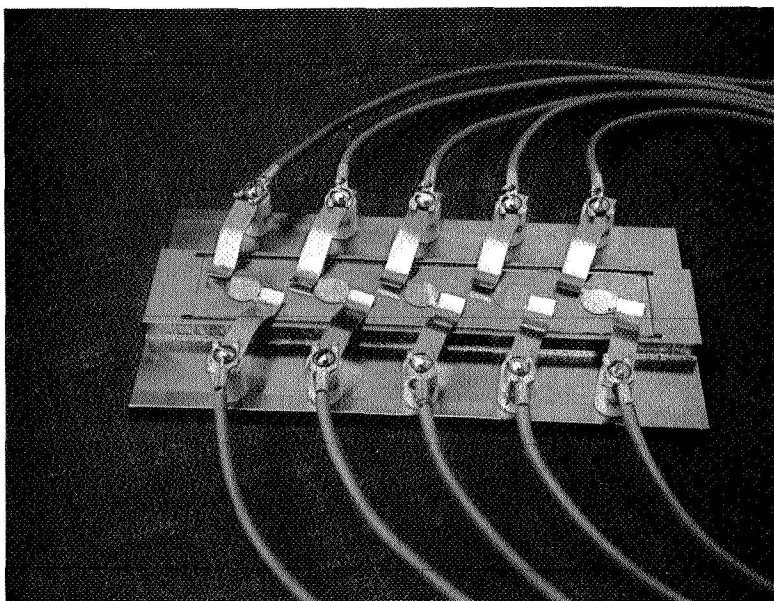


FIGURE 9. MULTIPLE-CAPACITOR LIFE TEST UNIT (Shown  
with Five Thin Film Capacitors in Position)

Typical silica sputtering runs were made as follows:

The system was first pumped to the  $10^{-8}$  Torr range and back-filled with argon to a pressure of approximately  $2 \times 10^{-3}$  Torr. This pressure was maintained in a dynamic system, with argon flowing into a sorption pump through a nearly closed valve. Titanium sublimation continued during the run to help purify the argon and to pump desorbed active gases. Two 750-turn magnets carrying 2.2 amperes produced a uniform magnetic flux density of 78 Maxwells per square centimeter in the position of the substrates when the plasma was off. This magnetic flux served to contain the plasma and increase its density. The rf voltage was approximately 850 volts. The reflected power reading of 0.25 corresponded to a standing-wave ratio of approximately 1.1. The power-amplifier grid current was 65 ma, and its plate current was 275 ma.

Although most of the silica deposits were made as above, magnet currents ranged from 2.0 to 2.4 amperes and the rf voltages ranged from 700 to 1000 volts. The other parameters varied only by a very small amount.

Aluminum. -- In a multilayer capacitor, each deposited layer must have a minimum surface roughness to prevent irregularities from being exaggerated, layer after layer. Specular reflectivity is a good measure of the smoothness of aluminum films. All vacuum evaporated aluminum films were excellent specular reflectors.

Aluminum films that were sputter deposited on 0.050-inch thick glass had good specular reflectance, but those deposited on thinner (0.008 to 0.010 inch) glass had a matte finish. The finish is bluish in color when surface roughness is moderate and chalky white when the surface is very rough. Figure 10 shows the difference between a specularly reflecting aluminum film and one with a matte finish. A rough surface is not unusual in sputter-deposited aluminum films and has been discussed by Cook *et al.* (Ref. 4) as well as by several others. The generally accepted cause is too high a substrate temperature, resulting in large crystallites.

It appears that the difference in specularity of aluminum films on substrates of different thicknesses is the result of the following mechanism. Both the thick and thin glass slides lie on the water-cooled substrate

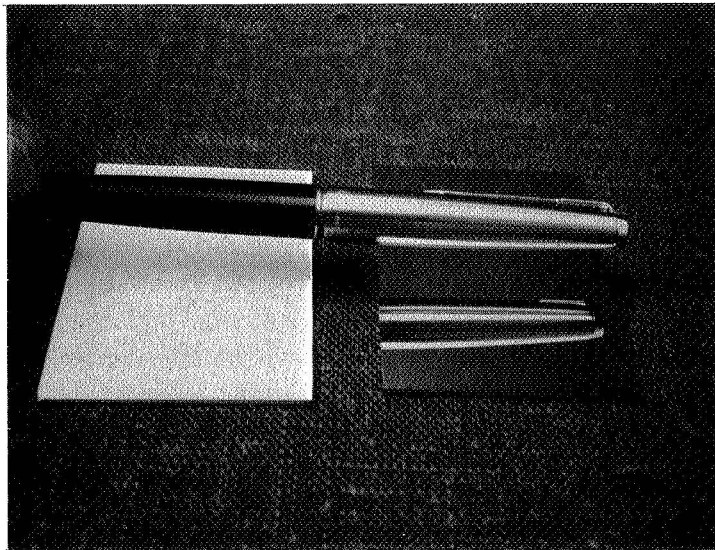


FIGURE 10. COMPARISON OF SPUTTERED ALUMINUM FILMS  
(Matte on left; Specular on right)

table under only the force of gravity. Thermal contact is poor, and the water cooling is largely ineffective. Both substrates absorb heat radiated by the target and by the plasma until a relatively thin film of aluminum has been deposited. Then the majority of this radiation is reflected, and the heat input by radiation drops significantly. The thicker substrate has enough heat capacity to keep the surface relatively cool until the radiation begins to be reflected. The thin substrate, on the other hand, has much less heat capacity, and its temperature rises high enough to foster the growth of large crystallites before the surface can become an effective heat reflector. Thus, the problem can be solved by sputtering more slowly (a less dense plasma), especially at the beginning of a deposit. Also, the magnetic field can be arranged to minimize heating from high-energy secondary electrons.

A technique involving the use of a gallium film between substrate and substrate table has been successfully utilized by Schaible and Maissel (Ref. 5). Heat transfer is definitely improved, but there is the problem of reaction between the gallium and the copper substrate table. A diffusion barrier could probably be utilized, but we chose the solution of less heat input by decreasing the magnetic flux density and thus, lowering the plasma density.

The system parameters for aluminum sputtering were very much like those for silica sputtering, except that the rf voltage was usually approximately 800 volts and the magnet current was 1.0 ampere. This produced a uniform magnetic flux density of 36 Maxwells per square centimeter in the position of the substrates when the plasma was off. This flux density, being lower than that used for dielectric deposition, allowed the substrate to remain cool enough to obtain a specularly reflecting aluminum film. Also, the aluminum target, 11.6 cm in diameter, was further from the substrate by 0.32 cm, the thickness of the silica target.

Silica-Aluminum Capacitors. -- The majority of test capacitors made during the conduct of this contract had aluminum electrodes and silica dielectrics. There were three basic configurations as shown in Figure 11 (a, b, and c). Most test capacitors were made in configuration a. The

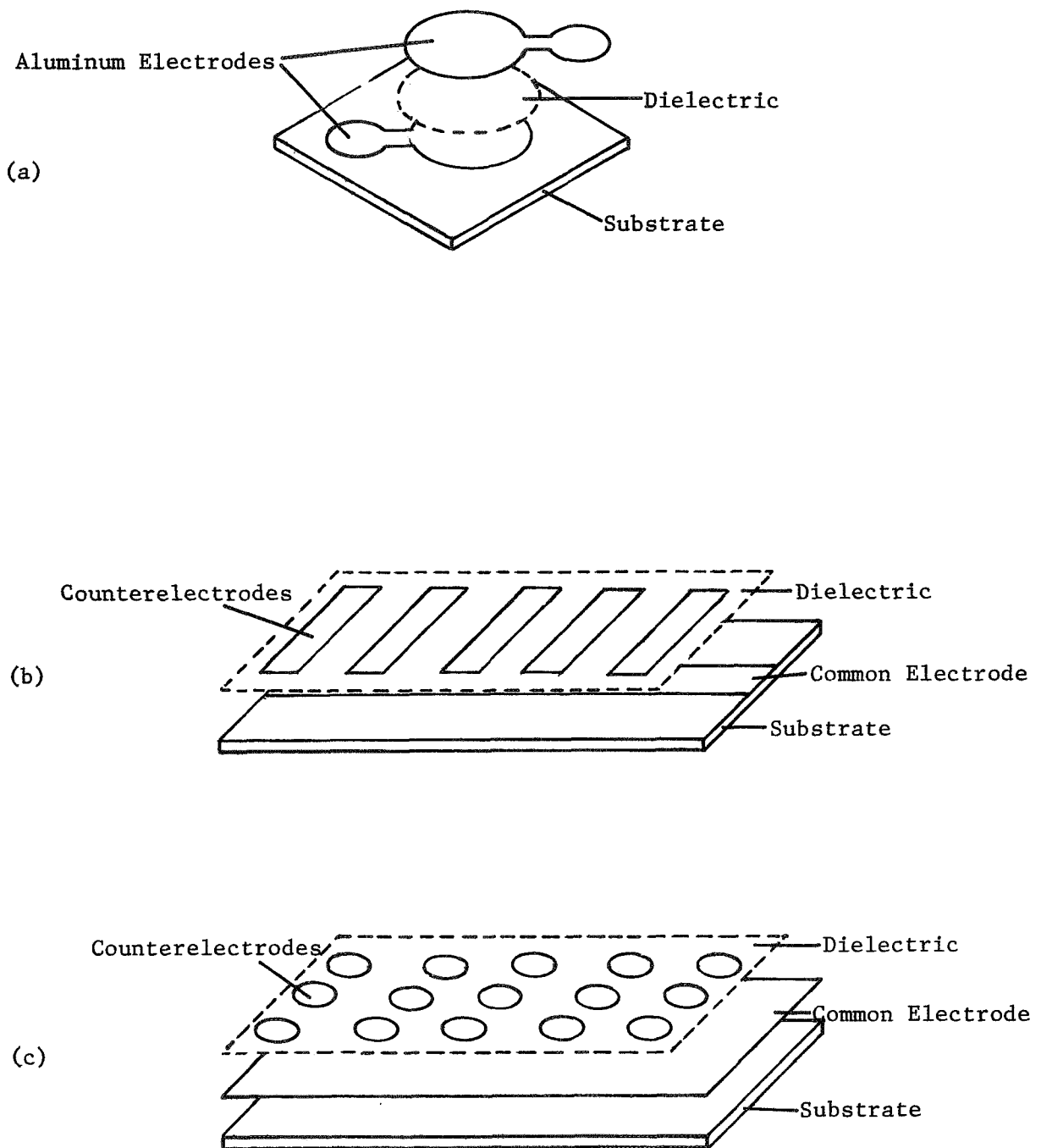


FIGURE 11. EXPERIMENTAL CAPACITOR ARRANGEMENTS

- a. 0.950-cm-diameter disk with contact tabs on 1.0-by-1.0-inch glass substrate
- b. Five 1/4-by-1/4-inch capacitors on 1-by-3-inch microscope slide.
- c. 1/4-inch disk capacitors on 1-by-3-inch microscope slide.

electrodes were deposited as 0.950-cm-diameter disks with a side arm for contact. The dielectric was deposited on the entire substrate except for the ends of the side arms. The side arms point in opposite directions on the odd- and even-numbered electrodes. Thus, when multiple layers were deposited, all the odd-numbered electrodes (and also the even-numbered electrodes) contacted each other through the void in the deposited dielectric.

The configurations shown in Figure 11 (b and c) were used for measurement of breakdown voltage versus dielectric thickness, and of dissipation factor versus electrode thickness. These arrangements yielded more capacitors per deposition than did the configuration in Figure 11 (a).

The number of layers that could be successfully deposited with the mask and target changer has not been determined. Without using the changer, ten capacitor layers appeared to be a practical limit. We believe that this limit is a result of the large amount of handling and the exposure to many pump-downs. The system had to be opened for each dielectric and each electrode layer, or 21 times for a 10-dielectric-layer capacitor. Any dust in the system (*e.g.*, deposited film that has flaked) is blown about during initial pumping, causing shorts that can be healed by application of a dc voltage that vaporizes the aluminum producing the short. After ten dielectric layers, there appears to be too many shorts to heal successfully. A tight-fitting shutter over the substrates during pump-down, as designed into the mask changer, would certainly increase the number of layers that could be deposited, even without the mask and target changer assembly.

Preferred film thicknesses for silica-aluminum capacitors were established as about 3000 Å for silica dielectric and 1500 Å for aluminum electrodes. The objective of high capacitance density dictates as thin a dielectric layer as possible, consistent with working voltage requirements. These voltage requirements were low enough to permit using dielectric layers somewhat less than 3000 Å thick. However, at thicknesses not much less than 3000 Å there is a noticeable decrease in yield -- the percentage of fabricated capacitors that are usable. A very rapid decline in yield at approximately 1000 Å was noted by Davidse and Maissel (Ref. 6). Improved

fabrication conditions (less handling and close-fitting shutter during pump-down) will accompany use of the mask and target changer. A high yield at somewhat thinner dielectric layers and, thus, at increased capacitance density, should result.

High capacitance density also requires the electrodes to be as thin as possible. There is a lower limit to the thickness of the electrodes, governed by the need to keep the dissipation factor low. One of the principal components of the total dissipation factor is the series resistance in the plane of the electrodes (Ref. 7). Aluminum electrodes have high conductivity but at 1000 Å thickness, there is a notable increase in dissipation factor. Many capacitors with 1200-Å-thick electrodes have had good dissipation factors, and it is possible that such a thickness could be used with the mask and target changer. Currently, 1500-Å-thick aluminum electrodes give reliably low dissipation factors.

Alumina-Aluminum Capacitors. -- The alumina test capacitors were made in the configurations shown in Figure 11 (a and c). These capacitors were either single or double-layer. Most of the alumina dielectric layers were approximately 3000 Å thick and the aluminum electrodes were 1200 to 1500 Å thick.

### Capacitor Tests

Dielectric Strength. -- The dielectric strength of the dielectric material determines the breakdown voltage of a capacitor. Given a fixed breakdown voltage requirement, the dielectric strength determines how thin the dielectric can be made and still meet the requirement.

The dielectric strength of bulk silica is  $1.6 \times 10^5 \text{ V cm}^{-1}$ , and for alumina, it is  $8.4 \times 10^4 \text{ V cm}^{-1}$ . The dielectric strengths of materials increase with decreasing thickness in film form. However, when they become very thin, minor film defects and surface roughness might cause a decrease in dielectric strength. Essentially all of the thin film silica capacitors had dielectric strengths in the  $10^6 \text{ V cm}^{-1}$  range. The results tabulated in Table I are typical and agree well with known values (Ref. 8).

TABLE I  
DIELECTRIC PROPERTIES OF  
SILICA-ALUMINUM CAPACITORS

Dielectric Thickness (A)	Mean Breakdown (V)	Standard Deviation of Breakdown (V)	Dielectric Strength (Vcm <sup>-1</sup> )
1090	34.25	7.91	3.14 x 10 <sup>6</sup>
2100	68.75	17.47	3.27 x 10 <sup>6</sup>
2920	93.75	27.09	3.21 x 10 <sup>6</sup>
3700	99.00	36.00	2.68 x 10 <sup>6</sup>
4930	243.75	19.23	4.93 x 10 <sup>6</sup>
5200	136.00	37.00	2.62 x 10 <sup>6</sup>
5200	288.75	56.43	5.54 x 10 <sup>6</sup>
6600	89.00	29.00	1.35 x 10 <sup>6</sup>
13200	348.00	81.00	2.64 x 10 <sup>6</sup>

Capacitance and Dissipation Factor. -- The two-terminal equivalent electrical circuit of a capacitor may be represented by a series resistance (R) and inductance (L) connected to a parallel combination of capacitance (C) and conductance (G), as shown in Figure 12. The series resistance and inductance represent the equivalent circuit of the connecting leads and electrodes of the capacitor. The capacitance exists between the capacitor plate electrodes, and the conductance represents the losses of the solid dielectric between the capacitor plates.

At low frequencies, the effects of the series resistance and inductance are negligible, and the capacitor acts as a pure capacitance in parallel with a conductance. As the frequency is increased, the inductance becomes an important consideration because a condition of resonance occurs between (L) and (C). For frequencies below resonance, the inductance partially neutralizes the effect of the capacitance, resulting in an effective terminal capacitance given approximately by the following equation. (Equations given in this section are derived in the Appendix).

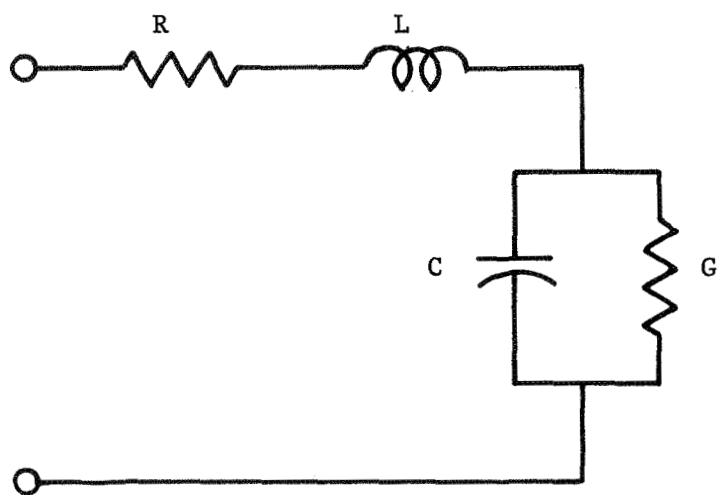


FIGURE 12. EQUIVALENT ELECTRICAL CIRCUIT OF A CAPACITOR

$$C_t = \frac{C}{1 - \omega^2 LC} \quad (1)$$

The dissipation factor for a capacitor is defined as the ratio of the energy dissipated to the energy stored. In terms of the equivalent circuit of Figure 12, the dissipation factor is given by:

$$D = \frac{R + \frac{G}{\omega^2 C^2 + G^2}}{\omega L - \frac{\omega C}{\omega^2 C^2 + G^2}} \quad (2)$$

At low frequencies, and for the case of a reasonably good capacitor, e.g.,

$$L = 0$$

$$G^2 \ll \omega^2 C^2$$

the total dissipation factor is

$$D = \omega CR + \frac{G}{\omega C} \quad (3)$$

For a solid dielectric capacitor, the dominant component of the conductance is the loss in the dielectric. The loss varies with frequency. The dissipation factor is directly proportional to the energy dissipated and is the sum of the three principal components.

1. A constant dissipation factor caused by residual polarization.
2. Interfacial polarization loss.
3. Series resistance in the leads and capacitor plates.

The total dissipation factor has a minimum value at a frequency that varies inversely with capacitance. The minimum usually occurs between 1 kHz and 1 MHz.

A typical result for the variation of dissipation factor with frequency for a silica dielectric capacitor is shown in Figure 13. The residual polarization results in a constant dissipation factor and would result in a horizontal line. The loss produced by interfacial polarization causes the slant downward to the right. This is overshadowed in most of the silica-aluminum capacitors by ohmic losses in the leads and plates that cause the slant upward to the right at high frequencies. The series resistance (R) is not usually significant at low frequencies. As the frequency is increased, the skin effect becomes significant, the resistance increases, and is a function of the square root of the frequency. This resistance relationship may be expressed as  $R_1 f^{1/2}$ , where  $R_1$  is the resistance at 1MHz and (f) is the frequency in megahertz. The total dissipation factor at high frequencies is then:

$$D = \frac{G}{\omega C} + R_1 f^{1/2} \omega C \quad (4)$$

At low frequencies, the only losses that are important are represented by the parallel conductance (G).

The dissipation factor versus frequency plot in Figure 13 is for a double-layer disk-shaped silica-aluminum capacitor (Figure 11a) at 22°C. The dissipation factor versus frequency for two six-layer silica-aluminum capacitors at 22°C is shown in Figure 14. The thickness of each dielectric layer on these capacitors is approximately 4200 Å, and electrode thicknesses are 1200 to 1400 Å. Capacitance versus frequency for these six-layer capacitors is plotted in Figure 15.

Capacitance and dissipation factors versus frequency and temperature were measured for a large number of test capacitors. The bulk of the capacitors that were fabricated and tested were double-layer, 0.950-cm-diameter silica-aluminum capacitors on 2.5 x 2.5 cm glass substrates. Capacitor XIV, from a series of these double-layer capacitors, had dielectric thicknesses of 3700 Å and electrode thicknesses of approximately 1200 Å.

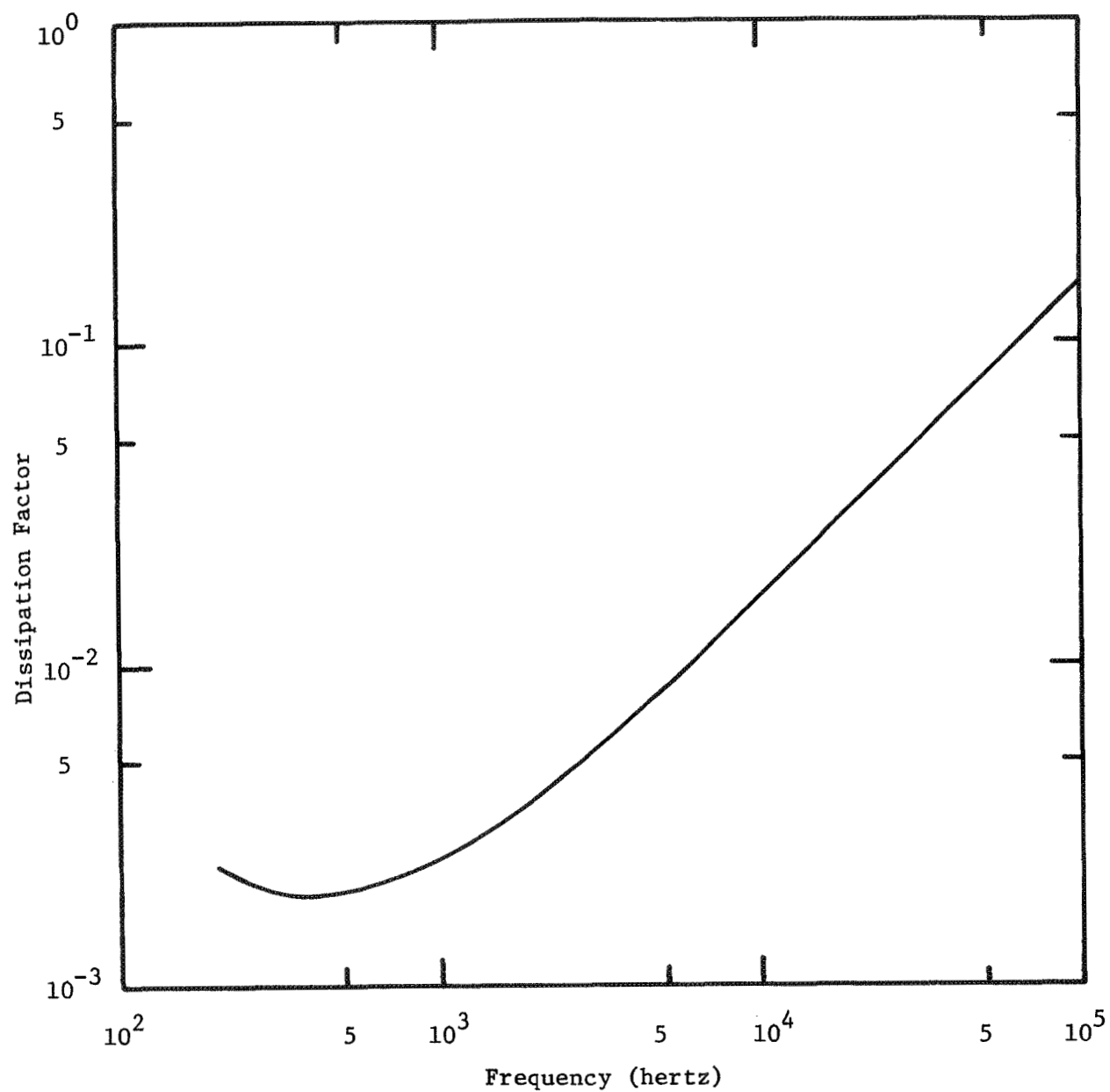


FIGURE 13. THE EFFECT OF FREQUENCY ON DISSIPATION FACTOR AT 22°C  
FOR A TYPICAL DOUBLE-LAYER SILICA CAPACITOR

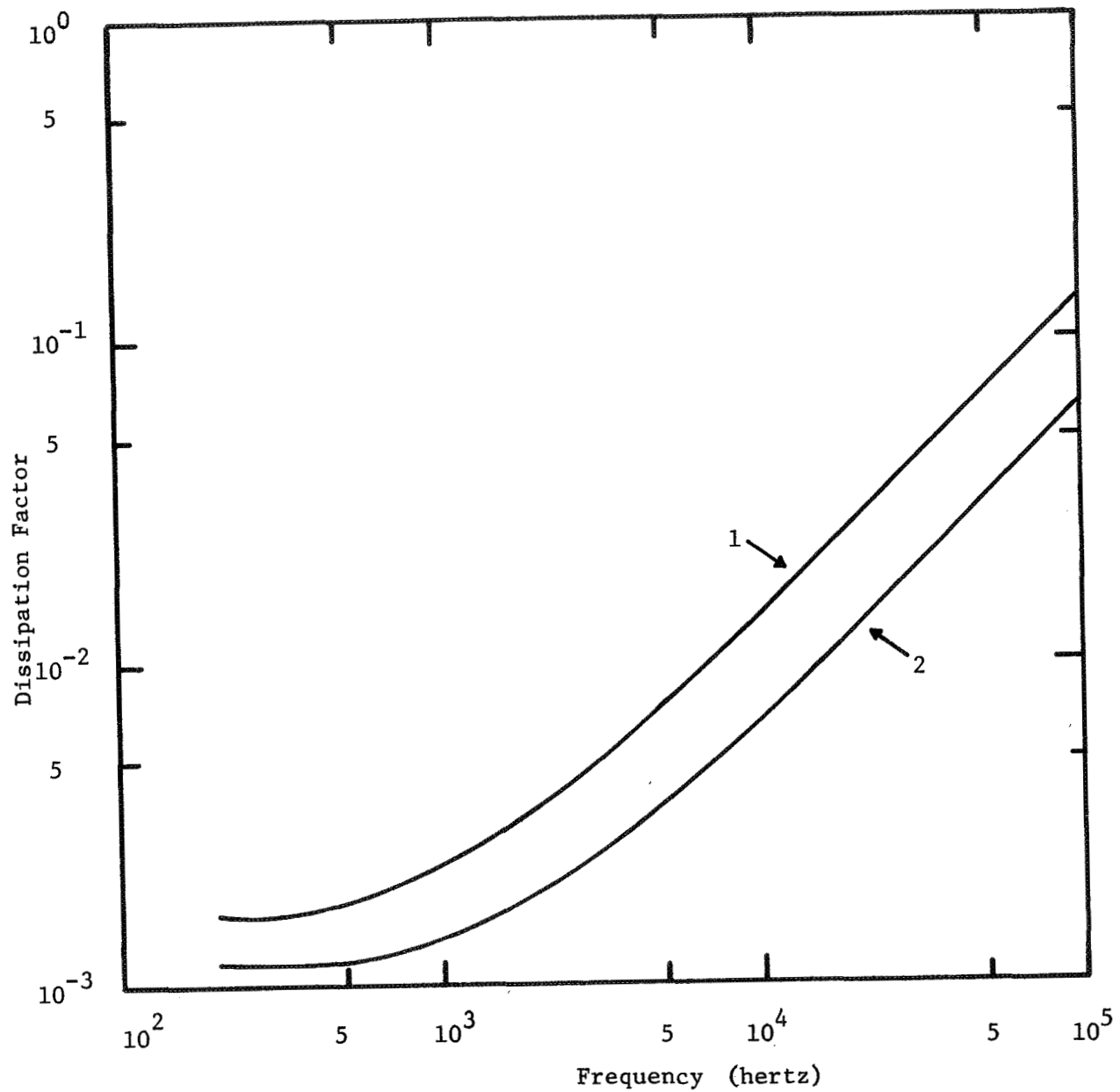


FIGURE 14. THE EFFECT OF FREQUENCY ON DISSIPATION FACTOR AT 22°C  
FOR TWO 6-LAYER SILICA-ALUMINUM CAPACITORS

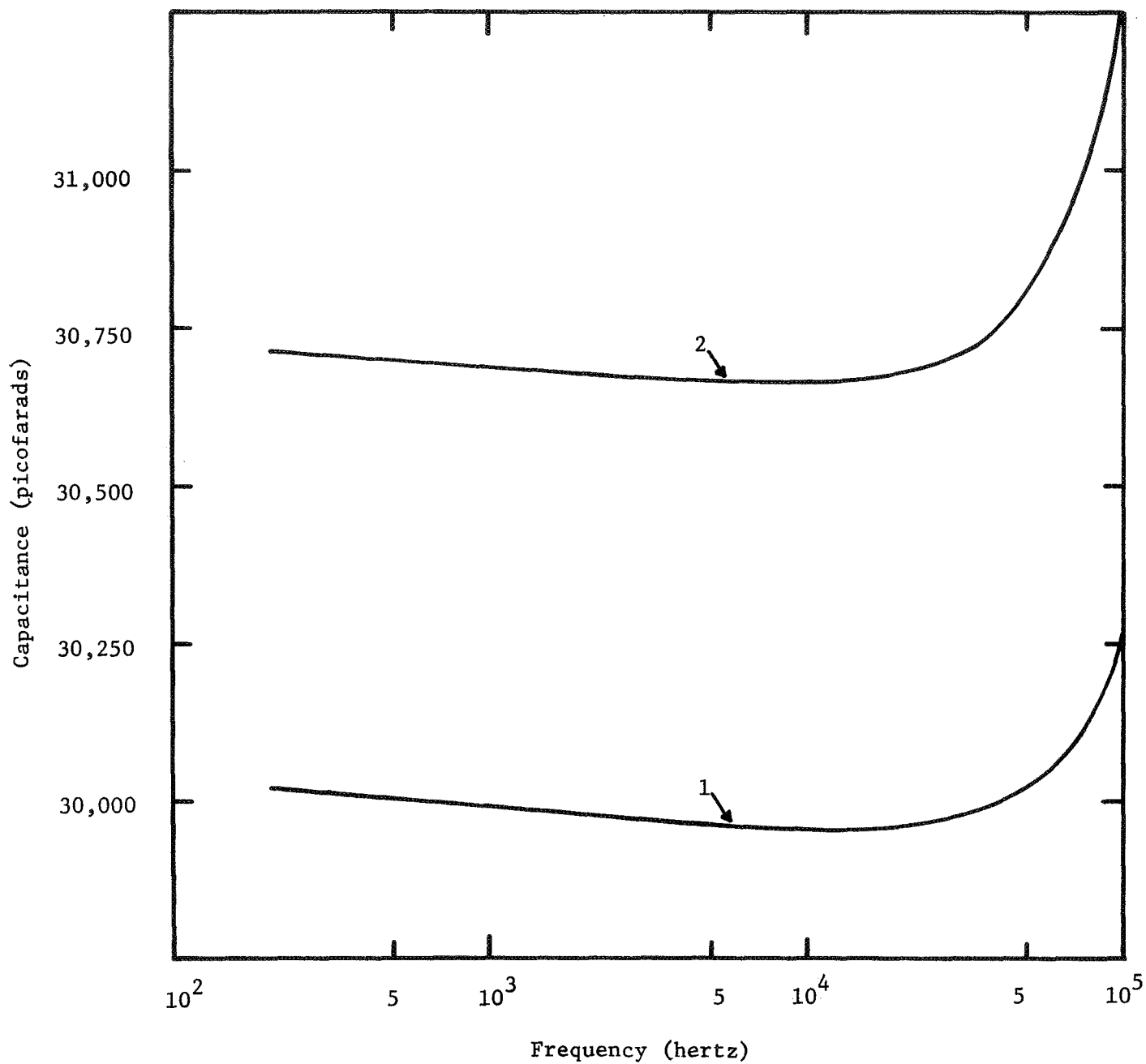


FIGURE 15. THE EFFECT OF FREQUENCY ON CAPACITANCE AT 22°C FOR TWO 6-LAYER SILICA-ALUMINUM CAPACITOR XIV

On most capacitors, including XIV, elevated-temperature life tests were performed first. This allowed the capacitor to come to an equilibrium condition before the other measurements were made. In some capacitors, electrical characteristics versus temperature were measured in the "as fabricated" condition. This has the drawback that the electrical characteristics undergo some change at elevated temperatures. The life tests are described in a later section of this report.

Capacitance versus frequency and temperature for capacitor XIV is plotted in Figure 16. The capacitance increases with temperature at all frequencies from 200 Hz to 100 kHz. Between 20 and 50 kHz, the capacitance begins to increase rapidly at all temperatures from -79 to 225°C. The variation in capacitance with frequency up to 20 kHz is less than 0.2 percent and, as the frequency is increased to 100 kHz, the capacitance varies by approximately 2.5 percent.

Dissipation factor versus frequency and temperature for Capacitor XIV is plotted in Figures 17 and 18. With the exception of the 25°C curve, the dissipation factor increases with increasing temperature at low frequencies. There is some indication that the dissipation factor decreases with increasing temperature at the high frequencies, but the curves tend to be close together because the dependence on temperature is much less pronounced. The dissipation factors of these capacitors compare very favorably with the range of  $5 \times 10^{-4}$  to  $10^{-3}$  at 1.0 kHz quoted by Augustine *et al.* (Ref. 9) for rf sputtered silica.

The effect of frequency and temperature on capacitance for alumina-aluminum capacitors is shown in Figure 19. This is from a series of single layer, 0.635-cm-diameter capacitors of the configuration shown in Figure 11 (c). The effect of frequency and temperature on dissipation factor for this same series is shown in Figure 20. Figures 19 and 20 show that the capacitance and dissipation factor of alumina-aluminum capacitors are very sensitive to temperature. This is the principal reason that nearly all the later work was with silica-aluminum capacitors.

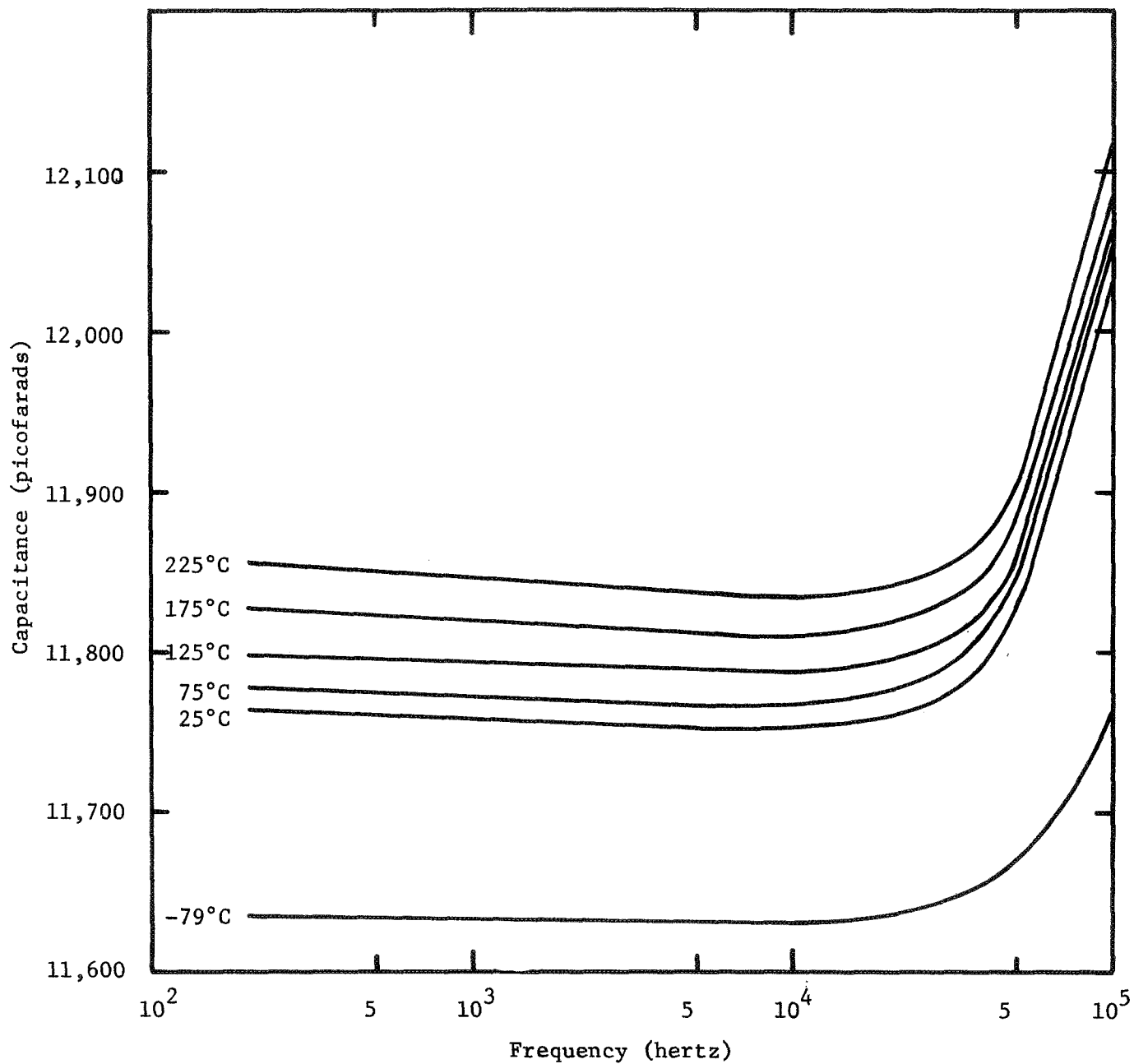


FIGURE 16. THE EFFECT OF FREQUENCY ON CAPACITANCE AT SEVERAL TEMPERATURES FROM -79 to 225°C FOR SILICA-ALUMINUM CAPACITOR XIV

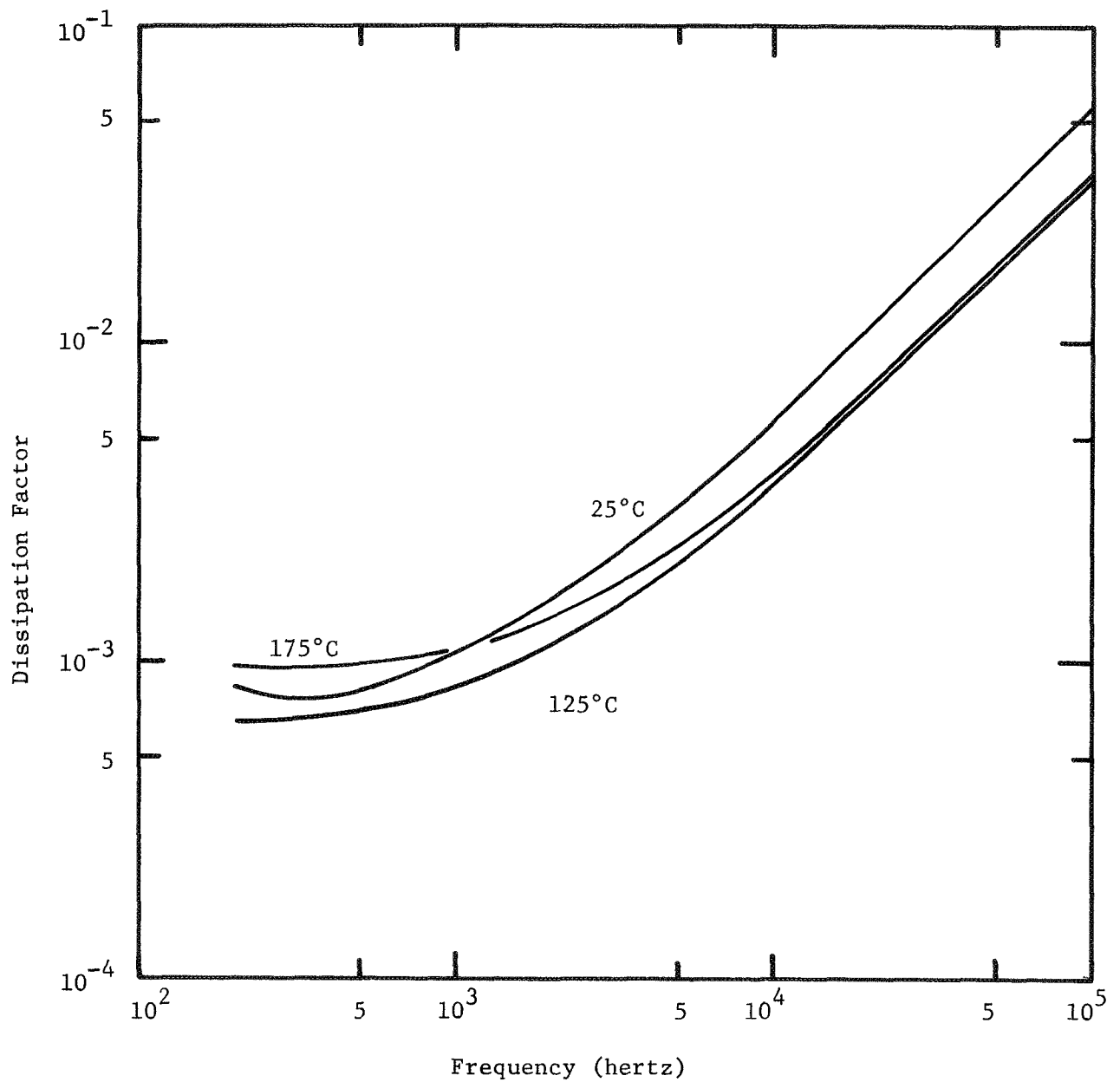


FIGURE 17. THE EFFECT OF FREQUENCY ON DISSIPATION FACTOR AT THREE TEMPERATURES FOR SILICA-ALUMINUM CAPACITOR XIV

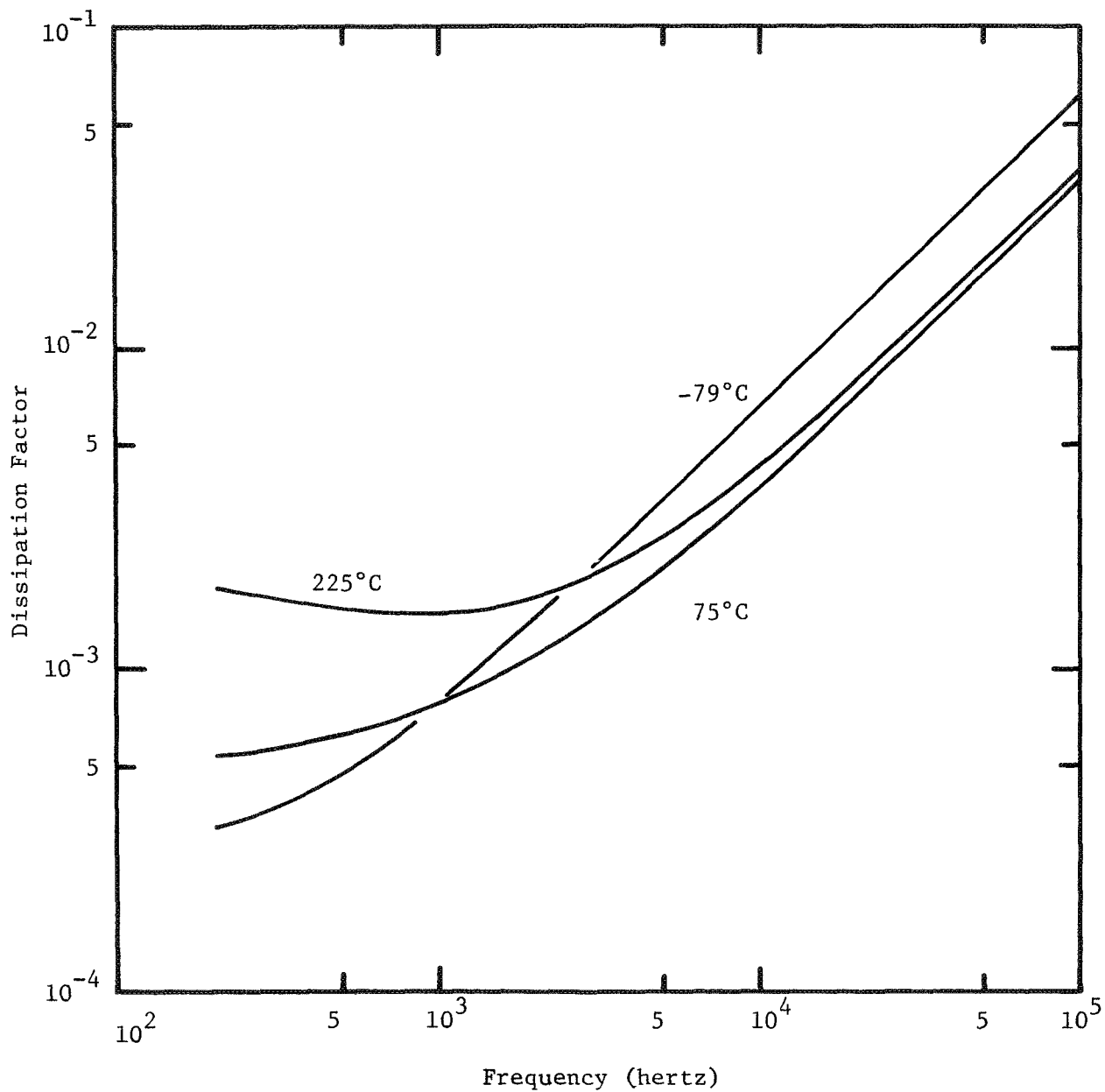


FIGURE 18. THE EFFECT OF FREQUENCY ON DISSIPATION FACTOR AT THREE TEMPERATURES FOR SILICA-ALUMINUM CAPACITOR XIV

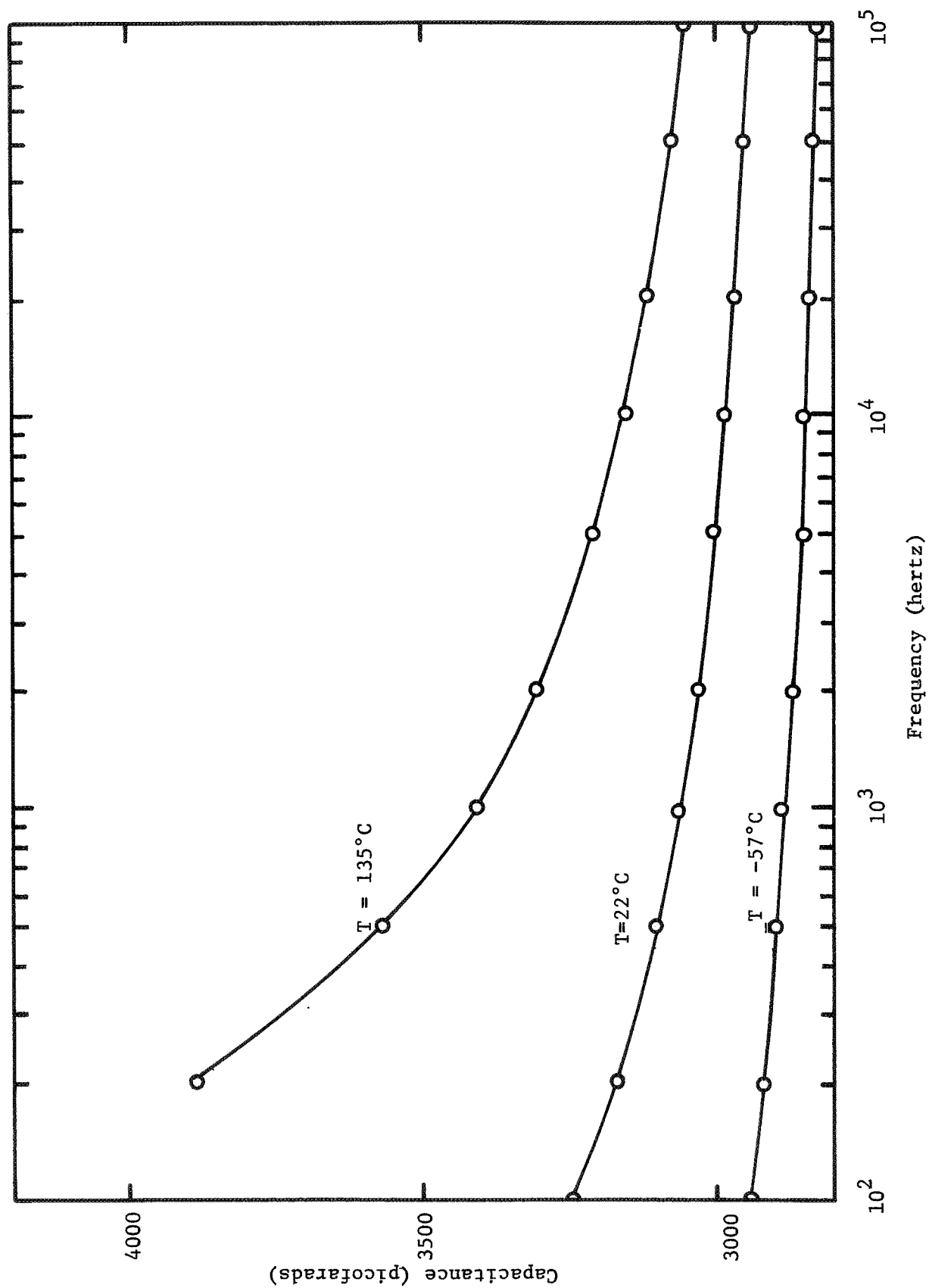


FIGURE 19. THE EFFECT OF FREQUENCY AND TEMPERATURE ON CAPACITANCE OF AN ALUMINA-ALUMINUM CAPACITOR

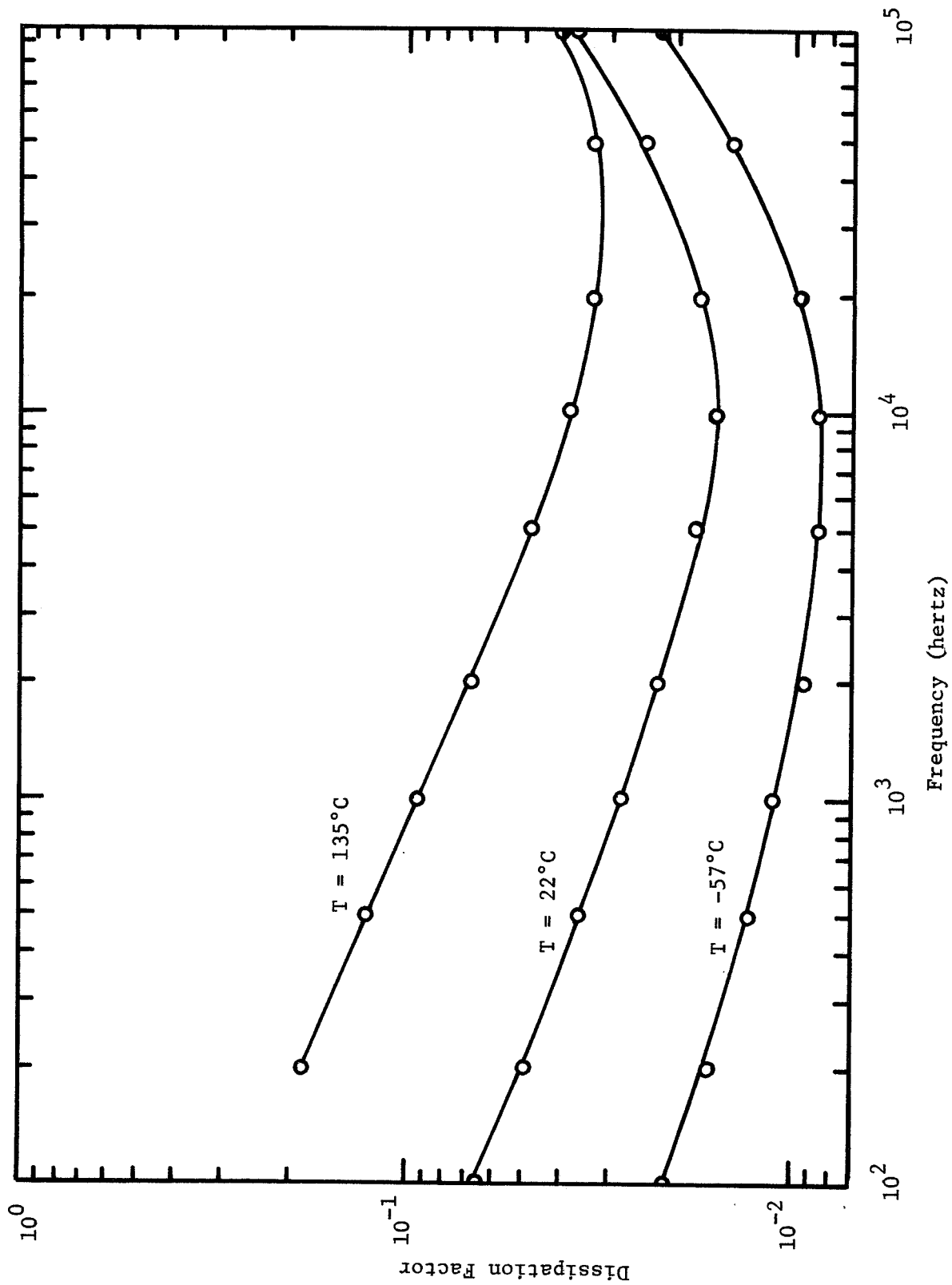


FIGURE 20. THE EFFECT OF FREQUENCY AND TEMPERATURE ON DISSIPATION FACTOR OF AN ALUMINA-ALUMINUM CAPACITOR

As was stated earlier, the measurements of capacitance and dissipation factor versus frequency and temperature were made after the capacitors had undergone a stabilizing bake-out in air. Figure 21 shows the change in capacitance versus frequency for a silica-aluminum capacitor effected by 312 hours at 150°C. The effect of the bake-out on dissipation factor versus frequency is shown in Figure 22. The rate of change of these electrical characteristics is discussed in the following section on life tests.

Measurements of dissipation factor versus electrode thickness were made on capacitors of the configuration shown in Figure 11 (b). A series of these five-capacitor substrates was produced with silica dielectric thicknesses of approximately 5000 Å and aluminum electrode thicknesses varying from 400 Å to 8600 Å. The measurements were made at 1.0 kHz and 100 kHz at 22°C. The results are plotted in Figure 23. Each point is the mean value for the five capacitors on one substrate. The bars include one standard deviation above, and one below, the mean values. These test capacitors were the first to be made entirely by sputtering silica and aluminum, which may be a contributing factor to the high degree of scatter in the results. Dissipation factors are also slightly higher at 1.0 kHz and much lower at 100 kHz than those shown in Figures 14, 17, and 22, for evaporated aluminum electrodes. The higher density generally exhibited by sputter deposited films over those deposited by evaporation can contribute to the lower high-frequency dissipation factors. From a practical standpoint, capacitors with sputter-deposited electrodes are better at high frequency because of the lower dissipation factor. They are also better in applications covering a range of frequencies because the dissipation factor is much less frequency dependent. There were no dissipation factors of more than  $10^{-2}$  at thicknesses over 1000 Å, even at 100 kHz. In spite of the scatter, it can easily be seen that the 1.0 kHz and 100 kHz dissipation factors converge as the electrodes get thicker. It appears that the ultimate value lies between  $2 \times 10^{-3}$  and  $4 \times 10^{-3}$ .

Information about the power dissipation characteristics of the silica-aluminum capacitors was obtained by measuring their dissipation factors at three AC current levels. The measurements were taken at several frequencies between one and 100 kHz. Currents were limited to small values because the voltages had

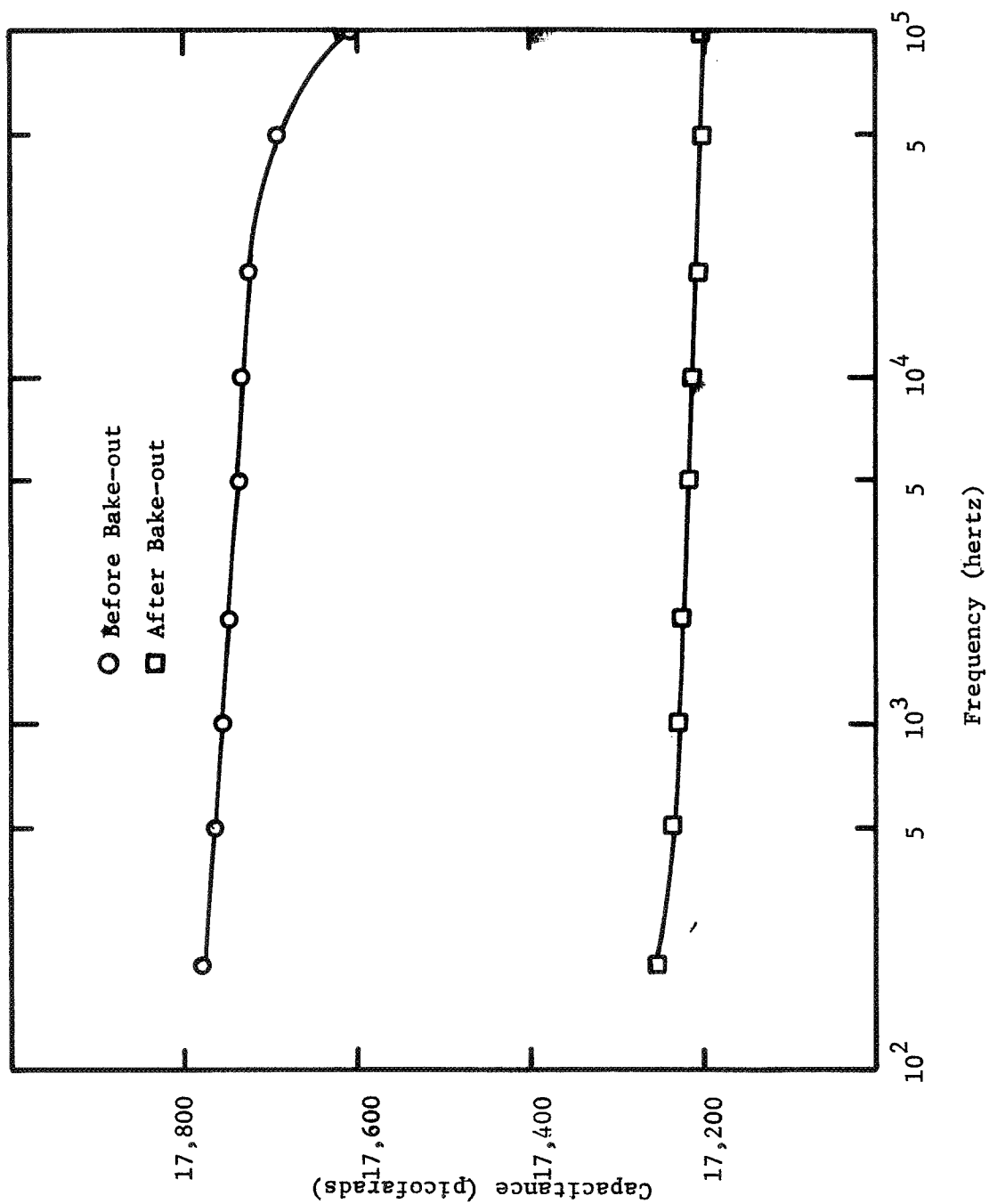


FIGURE 21. THE EFFECT OF 312 HOURS EXPOSURE TO 150°C IN AIR ON THE FREQUENCY-CAPACITANCE RELATIONSHIP (Double-Layer Silica-Aluminum Capacitor)

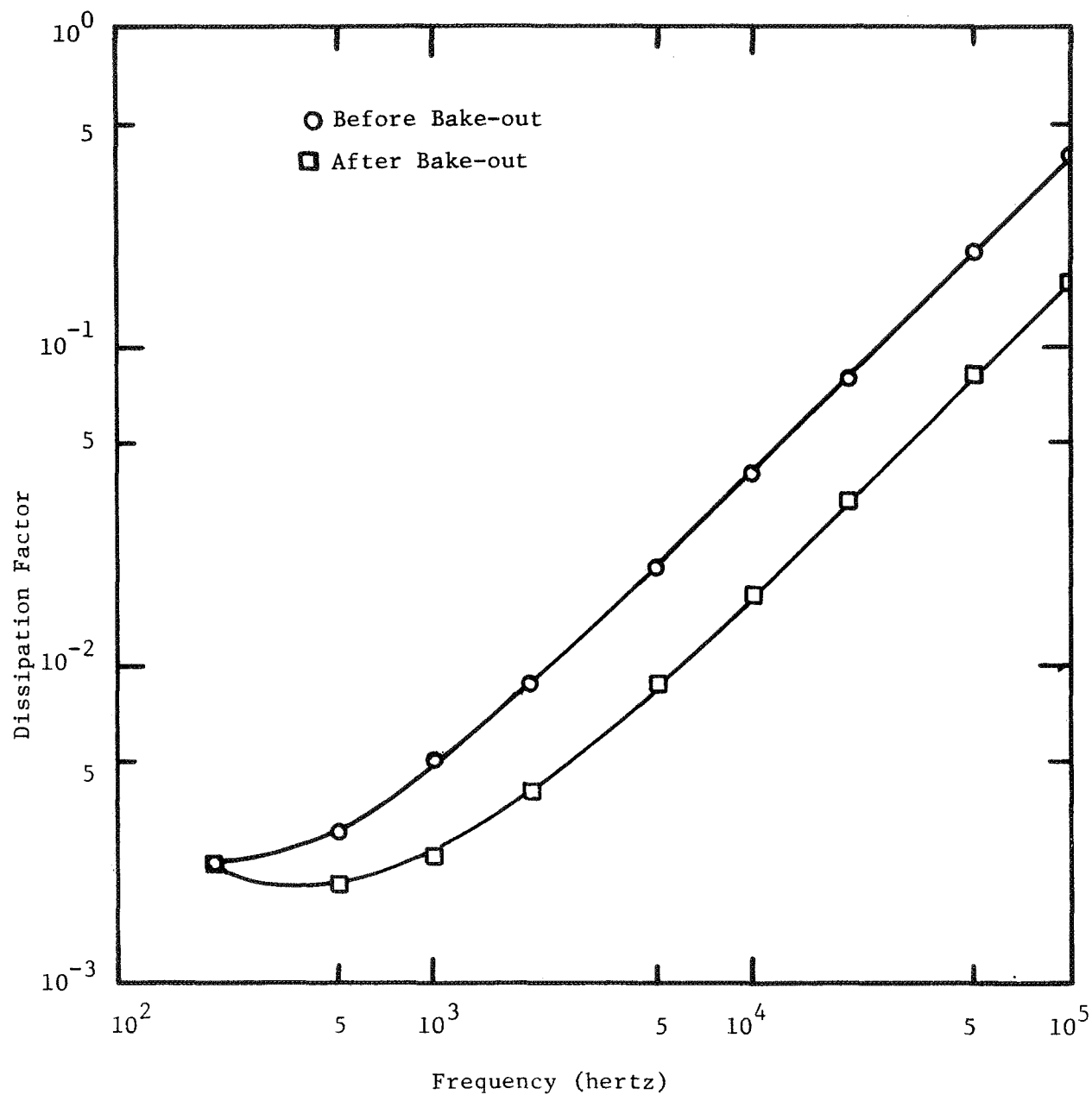


FIGURE 22. THE EFFECT OF 312 HOURS EXPOSURE TO 150°C IN AIR ON THE FREQUENCY-DISSIPATION FACTOR RELATIONSHIP (Double-layer silica-aluminum capacitor)

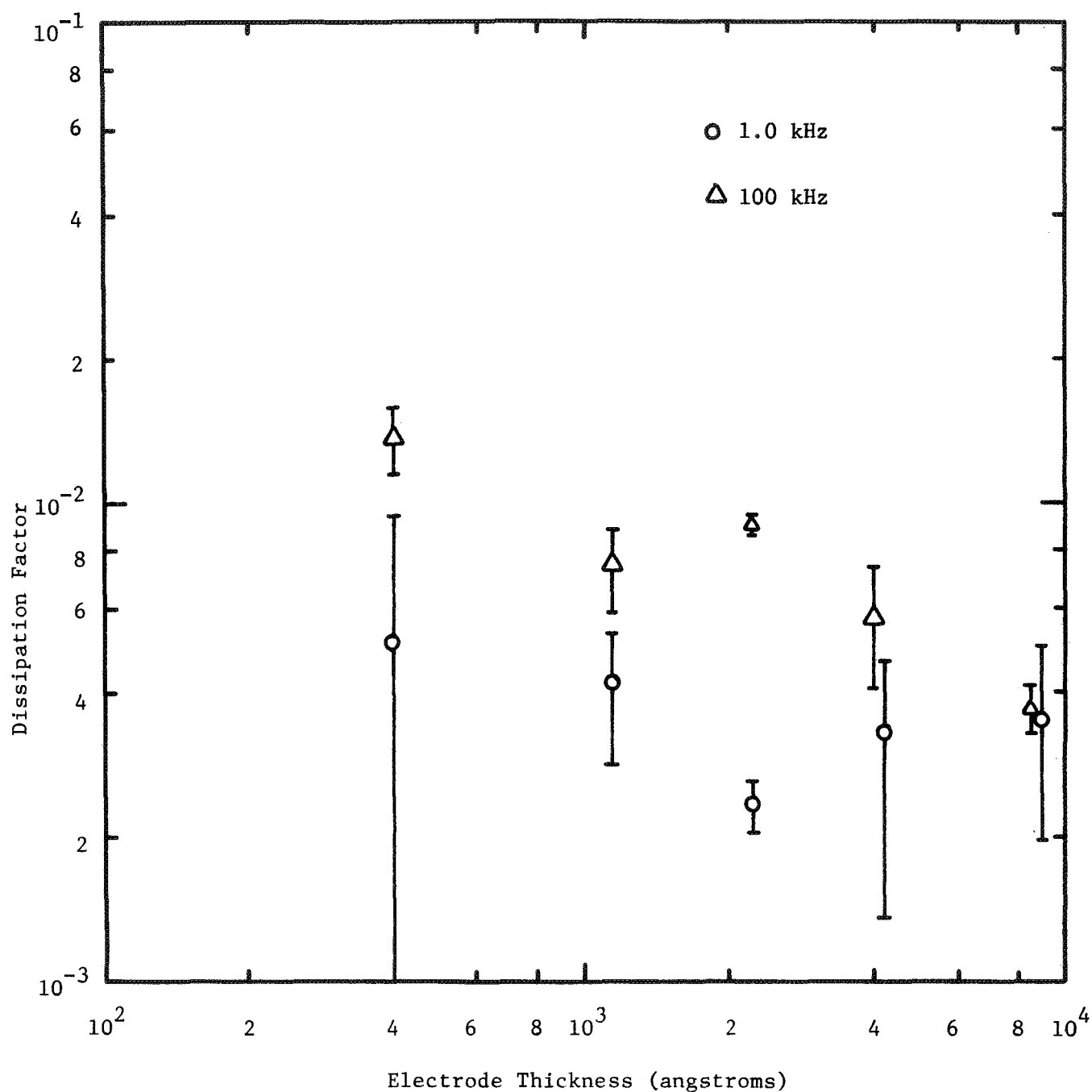


FIGURE 23. MEAN VALUES OF THE DISSIPATION FACTOR FOR SILICA-ALUMINUM CAPACITORS AS A FUNCTION OF ELECTRODE THICKNESS AT 1.0 AND 100 kHz. (The error bars indicate one standard deviation above and one below the mean.)

to be kept well below the breakdown voltage. Dissipation factors were measured at 0.2 and 0.4 ma in addition to the current at which the original dissipation factor measurements were made. It is not known exactly what the currents were in the original measurements because they varied as a bridge circuit was nulled. However, they were lower than the 0.2 and 0.4 ma currents by at least two orders of magnitude. Figure 24 shows dissipation factor versus frequency for the very low current and for 0.2 and 0.4 ma. It can be seen that the dissipation factor is independent of the current, at least up to 0.4 ma, and thus the capacitor's operation will be unaffected by variations in the current up to 0.4 ma.

Life Tests. -- All life tests were carried out at -79°, 150, and 250°C. There does not appear to be any change in capacitance of double-layer silica-aluminum capacitors during exposure to -79°C, but there is a very small increase in the dissipation factor. Even though the capacitors were potted, this small increase in dissipation factor appears to result from condensation on the leads and on the surface of the potting compound.

Exposure of double-layer test capacitors to 150°C produced a small change in capacitance and dissipation factor in some capacitors (Figures 21 and 22), but for most capacitors there was essentially no change in capacitance or dissipation factor over a period of several hundred hours. At 250°C, there was a decrease in capacitance. The decrease was greater for low frequency than for high frequency, as shown in Figure 25. Note also that the capacitance changes very rapidly at first and then levels off to its final value. When these capacitors are returned to room temperature, their capacitance is lower than before the high-temperature exposure. Subsequent excursions to 250°C do not cause additional changes in the capacitance. Thus, part of the production procedure for these capacitors will have to be an air bake at the highest temperature at which the capacitors will be used. The duration of the bake might be reduced by baking at even higher temperatures, but this has not been established at this time.

Figure 26 shows percentage change in dissipation as a function of time at 25°C for a double-layer silica-aluminum capacitor. There is very little change at the highest frequency. At the lower frequencies there is a rapid decrease

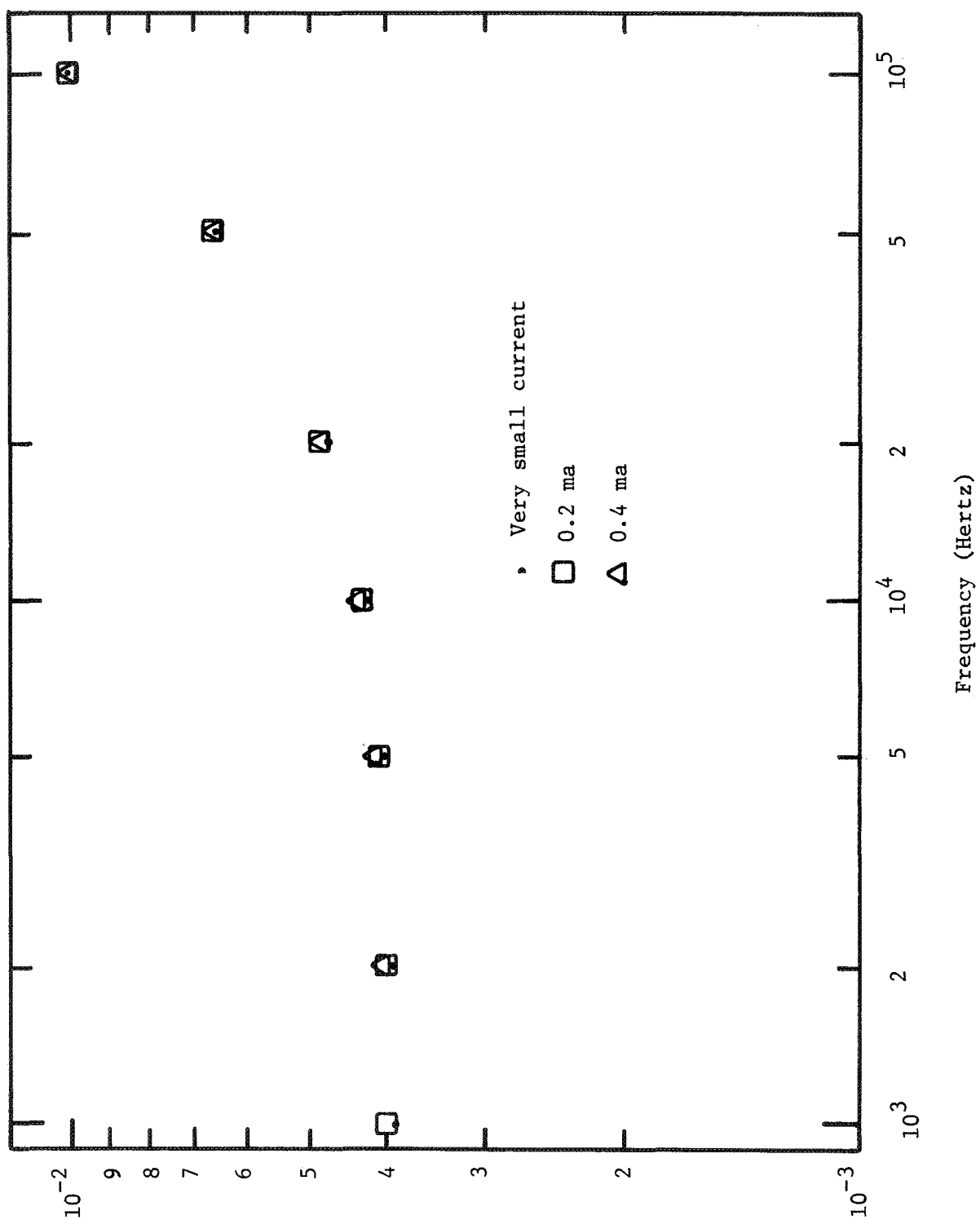


FIGURE 24. DISSIPATION FACTOR AS A FUNCTION OF FREQUENCY AND CURRENT

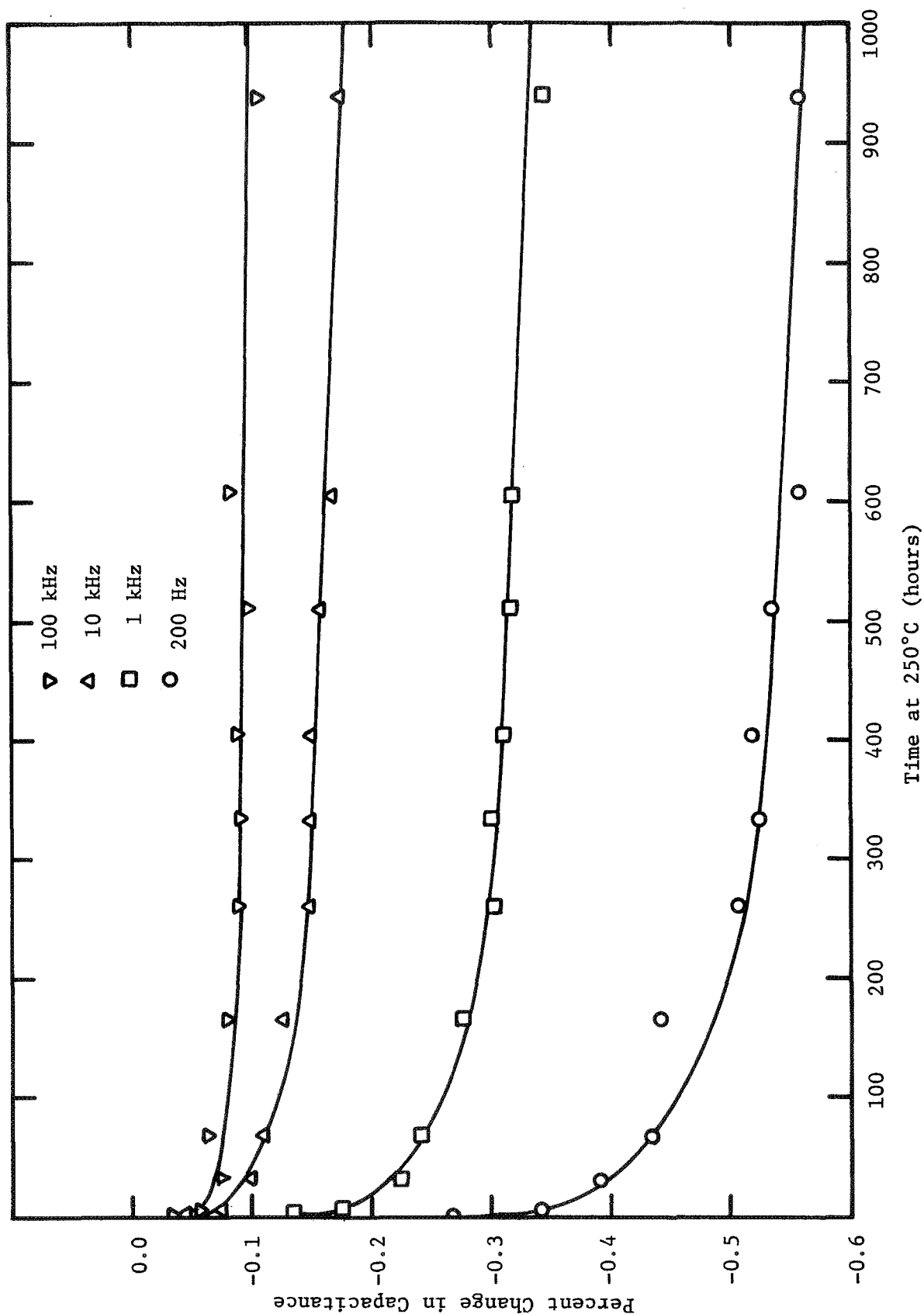


FIGURE 25. THE EFFECT OF LONG-DURATION, HIGH-TEMPERATURE EXPOSURE ON A SILICA-ALUMINUM CAPACITOR AT FOUR FREQUENCIES

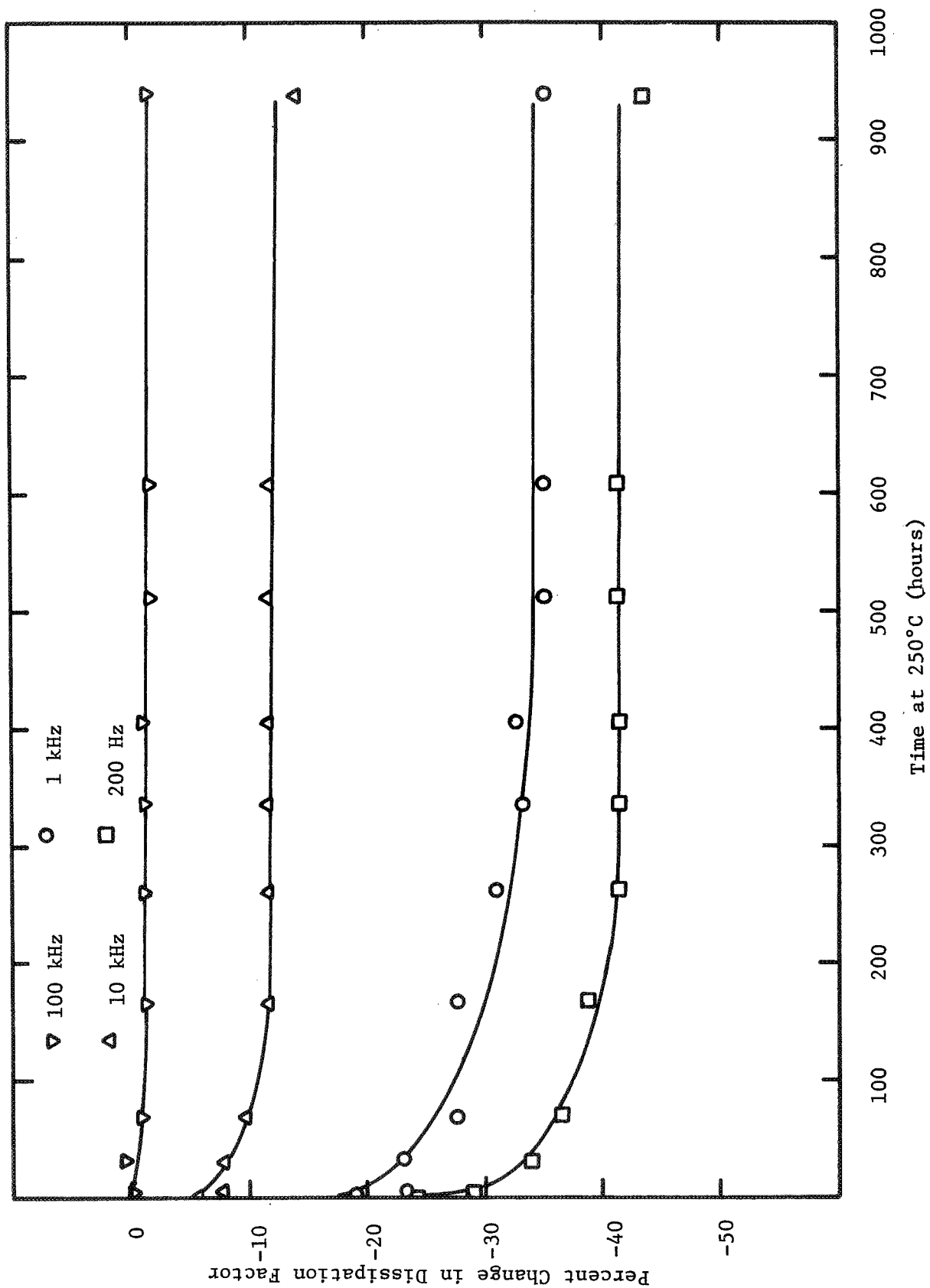


FIGURE 26. THE EFFECT OF 1000 HOURS EXPOSURE OF A DOUBLE-LAYER SILICA-ALUMINUM CAPACITOR TO 250°C IN AIR

in dissipation factor at first. The rate then levels off as it did for capacitance. The fact that the dissipation factor decreases with the air bake means that the capacitor has improved (has become less lossy). This indicates that minor defects in the dielectric layer have healed.

## CONCLUSIONS AND RECOMMENDATIONS

Thin metal- and oxide-film capacitors with high capacitance per unit volume and excellent electrical characteristics at elevated temperature can be deposited by low energy rf sputtering. Of the test capacitors that have been made, those that have the best electrical characteristics and the highest thermal stability are those with silica dielectrics and aluminum electrodes. The process has yielded capacitors with 320  $\mu\text{f}$  capacitance per cubic centimeter of deposited material. In a packaged capacitor of this type, 10  $\mu\text{f cm}^{-3}$  could probably be achieved. The dissipation factor of these capacitors is generally between  $5 \times 10^{-4}$  and  $5 \times 10^{-2}$ . Following a bakeout in air at 250°C, the capacitance of these capacitors varies only 0.6 percent from 25 to 250°C, and they are operable from -79 to 500°C. These values for capacitance density, dissipation factor, and high temperature capability are significant improvements over presently available capacitors whose corresponding values would be approximately 0.25  $\mu\text{f cm}^{-3}$ ,  $2 \times 10^{-4}$ , and 200°C, respectively.

Silica and aluminum can be sputter deposited readily to form capacitors of up to ten layers (ten dielectric layers and eleven electrode layers). More layers could be added by alternately depositing the two materials without breaking vacuum, thus greatly reducing the exposure of the substrate to contamination as a result of excessive handling. A mask- and target-changer system for fabricating multilayer capacitors without breaking vacuum has been designed and constructed; however, time did not allow it to be evaluated. When these capacitors are fabricated in a system that does not need to be opened between deposition steps, they will be a significant advance in capacitance density combined with excellent thermal stability and low power dissipation.

It is recommended that additional work be conducted to fabricate multilayer test capacitors using the new mask and target changer. When the maximum number of layers that can be stacked reliably has been established, the possibility of depositing that number of layers on each side of a substrate should be investigated. This would nearly double the capacitance per mass and per volume, because a rigid substrate is still the largest contributor to mass and volume.

When the problems associated with depositing multilayer capacitors without breaking vacuum have been worked out, techniques that are employed should be engineered into a production process.

It is also recommended that capacitors be fabricated by rf sputtering other dielectric materials with much higher dielectric constants. This would allow higher capacitance per volume in applications that do not require the high-temperature stability of silica. For a high charge storage density, it would be necessary to find a material with high dielectric constant and low dissipation factor that could be utilized in the multilayer thin film form.

## REFERENCES

1. Vromen, B.H., and Gerstenberg, D., Proc. 1968 IEEE, Electronic Components Conference, pp. 145-51 (May 8-10, 1968).
2. Pitt, K.E.G., *Vacuum*, 17, No. 10, p. 560 (October 1967).
3. Anderson, D.C., *Research/Development*, 19, p. 46 (January 1968).
4. Cook, H.C., Covington, C.W., and Libsch, J.F., *Trans. of Met. Soc. of AIME*, 236, pp. 314-320 (March 1966).
5. Schaible, P.M., and Maissel, L.I., *Thin Solid Films*, 3, p. 284, (1969).
6. Davidse, P.D., and Maissel, L.I., *J. Appl. Phys.*, 37, No. 2, p. 574 (February 1966).
7. Browning, M.E., Jorgenson, G.V., and Graves, W.H., First Interim Scientific Report, NASA Contract NAS 12-551 (June 1968).
8. Maissel, L.I., *Physics of Thin Films*, 3, G. Hass and R. Thun, eds., Academic Press, New York, p. 113 (1966).
9. Augustine, E., Hall, P., and Rossmeisl, R., "Properties of RF Sputtered Silicon Dioxide and Aluminum Oxide", *Proc. 5th Annual Elect. Symp.*, St. Louis (1966).

## New Technology Appendix

### MULTI-TARGET SPUTTERING APPARATUS

A description and figures relating to this invention are found on pages 9 through 13 of this report under the title "Mask and Target Changer".

This invention makes it possible to sputter-deposit more than one material without breaking vacuum. This is accomplished by moving new sources of material into position in front of the rf sputtering electrode. Commercially available systems for sputter-depositing more than one material without opening the vacuum system use a separate rf electrode for each material.

## APPENDIX

The equivalent electrical circuit of a capacitor is shown in Figure 12 and the terminal impedance is,

$$Z_t = (R + j\omega L) + \frac{1}{G + j\omega C} \quad (A-1)$$

Rearranging Equation (A-1) into real and imaginary components results in,

$$Z_t = R + \frac{G}{\omega^2 C^2 + G^2} + j \left( \omega L - \frac{\omega C}{\omega^2 C^2 + G^2} \right) \quad (A-2)$$

For,

$$G^2 \ll \omega^2 C^2$$

the effective terminal capacitance ( $C_t$ ) can be determined,

$$-\frac{1}{\omega C_t} = \omega L - \frac{1}{\omega C} \quad (A-3)$$

and

$$C_t = \frac{C}{1 - \omega^2 LC} \quad (A-4)$$

The dissipation factor (D) of the capacitor is the ratio of the magnitudes of the real and imaginary parts of Equation (A-2). At low frequencies, ( $L = 0$ ), and for  $G^2 \ll \omega^2 C^2$ ,

$$D = \omega CR + \frac{G}{\omega C} \quad (A-5)$$

DISTRIBUTION LIST  
FINAL REPORT

Contract Number NAS 12-551

National Aeronautics and Space  
Administration

Lewis Research Center  
21000 Brookpark Road  
Cleveland, Ohio 44135  
Attn: Mr. C.C. Conger (1)  
MS 54-1  
  
Mr. Robert English (1)  
500-201  
  
Mr. E.W. Otto (1)  
MS 54-1  
  
Dr. F.C. Schwarz (30)  
MS 54-5

Langley Research Center  
Hampton, Virginia 23365  
Attn: Mr. Merton Sussman (1)  
Bldg. 1202, Mail Stop 472

Goddard Space Flight Center  
Greenbelt, Maryland 20771  
Attn: Mr. McKenzie (1)  
Code 716.3

Manned Space Flight Center  
Houston, Texas 77501  
Attn: Mr. F.E. Eastman (1)  
Code EE4  
  
Mr. W.E. Rice (1)  
Code EP5

George C. Marshall Space Flight Center  
Huntsville, Alabama 35812  
Attn: Mr. R. Boehme (1)  
Code PD-DO-EP  
  
Mr. Robert Aden (1)  
Code S&E-ASTR-E

Jet Propulsion Laboratory  
4800 Oak Grove Drive  
Pasadena, California 91103  
Attn: Mr. Hubert M. Wick (1)  
Space Power Section  
  
Mr. T. Macie (1)  
Bldg. 122/123  
  
Mr. Alden Schloss (1)  
Bldg. 198/220  
  
Dr. F.T. Casal (1)  
NASA/Mission Analysis Division  
OART Mail Stop 202-8  
Moffett Field, California 94035

National Aeronautics and Space  
Administration  
Washington, D.C. 20545  
Attn: Mr. C.W. Harper (RD-A) (1)  
  
Mr. James Lazar (RNT) (1)  
  
Mr. Herbert D. Rothen (1)  
(RNP)  
  
Mr. P.T. Maxwell (RNW) (1)  
  
Mr. Charles H. Gould (RE) (1)  
  
Mr. A.J. Evans (RA) (1)  
  
Dr. F. Schulman (RNP) (1)  
  
Col. Ralph I. Larock (1)  
(RFS)  
  
Mr. A.O. Tischler (RP) (1)  
  
Mr. R.D. Ginter (RF) (1)

Flight Research Center  
Edwards, California 93523  
Attn: C.T. Johnson, Code A (1)

NASA Scientific and Technical Information Facility Attn: Acquisitions Branch (-AK/DL) P.O. Box 33 College Park, Maryland 20740	(2)	Naval Facilities Engr. Command Nuclear Power Division Washington, D.C. 20390 Attn: Mr. E. Morris Howard	(1)
Naval Air Systems Command AIR 53682 Department of Navy Washington, D.C. 20360 Attn: Mr. E. White	(1)	Mr. Myron Lowe, Code SS 310 Federal Aviation Agency 800 Independence Ave., S.W. Washington, D.C. 20553	(1)
Naval Air Development Center Johnsville Warminster, Pa. 18974 Attn: Mr. J. Segrest, AETD	(1)	Mr. Robert C. Hamilton IDA-Room 19, 9th Floor 400 Army-Navy Drive Arlington, Virginia 22202	(1)
Naval Air Test Center Patuxent River, Maryland 20670 Attn: Mr. T.P. Wilson, WST	(1)	Naval Air Systems Command AIR 5335 Department of the Navy Washington, D.C. 20360 Attn: Mr. Ohil Binderman	(1)
USAECOM AMESEL-KL-PG Fort Monmouth, N.J. 07703 Attn: Mr. Frank J. Wrublewski Mr. Robreski	(1) (1)	Mr. Jacob A. Adams ASBEP USAF Wright Patterson Air Force Base Ohio 45433	(1)
SEPO Division of Space Nuclear Systems Washington, D.C. 20545 Attn: Mr. Gerald Leighton	(1)	Mr. L. Cobb AETD, AEE Division Naval Air Development Center Johnsville, Pa., 18974	(1)
Commanding Officer U.S. Army MERDC Systems Application Division SMEFB-BD Fort Belvoir, Va. 22060 Attn: Mr. L. Gaddy, Jr.	(1)	Mr. E. Ward High Speed Ground Transportation Federal Railroad Administration Department of Transportation Washington, D.C. 20553	(1)
Mr. George Sherman (APIE) Chief, Aerospace Power Division Air Force Aero Propulsion Lab Wright Patterson Air Force Base Ohio 45433	(1)	Mr. Opeka Chief, Electro/Mechanical Branch SM-140 800 Independence Avenue, S.W. Washington, D.C. 20553	(1)
Mr. Richard L. Verga AIPE-2 Aero Propulsion Laboratory Wright Patterson Air Force Base Ohio 45433	(1)	National Institutes of Health Physical Sciences Administrator Bethesda, Maryland 20014 Attn: Mr. Roger S. Powell	(1)
Mr. B.J. Wilson, Code 5222 Naval Research Laboratory Washington, D.C. 20390	(1)		

## Other Recipients

TRW Systems Group One Space Park Redondo Beach, California 90278 Attn: Mr. A.D. Schoenfeld Bldg. 60/1160	(1)	Mr. Henry Johnson AC Electronics, Defense Research Laboratories GM Corporation 6767 Hollister Ave. Goleta, California 93107	(1)
VARO Static Power Division 1600 Dallas North Parkway Plano, Texas 75074 Attn: Mr. W.L. McNair	(1)	Mr. O.H. Preston Unit 251780 L.T.V. Aerospace P.O. Box 5907 Dallas, Texas 75222	(1)
Engineered Magnetics 13041 Cerise Avenue Hawthorne, California 90250 Attn: Mr. B. McComb	(1)	Comsat Laboratories Communications Satellite Corp. Box 115 Clarksburg, Md. 20734 Attn: Mr. Esch, Spacecraft Laboratory	(1)
AiResearch Manufacturing Co. 2525 West 190th Street Torrance, California 90509 Attn: Mr. K.M. Chirgwin	(1)	Mr. Esrom Day Fairchild Hiller Space and Electronic Systems Division Fairchild Drive Germantown, Md. 20767	(1)
Hamilton Standard Electronics Dept. Windson Locks, Conn. 06096 Attn: Mr. R.E. Sullivan	(1)		
Consolidated Avionics 800 Shames Drive Westbury, N.Y. 11590 Attn: Mr. G. O'Sullivan	(1)	Mr. Lionel Boulet Director, Hydro-Quebec Research Institute c/o Hydro Quebec Montreal, Canada	(1)
Dr. F. Storm General Electric Co. Research and Development Center P.O. Box 8 Schenectady, N.Y. 12301	(1)	Dr. A.E. Fitzgerald Dean of Faculty Northeastern University 360 Huntington Avenue Boston, Mass. 02115	(1)
Mr. V.J. Wattenburger General Electric Co. UFSTC Box 8555 Philadelphia, Pa. 19101	(1)	Dr. H.H. Woodson Professor of Electrical Engineering Massachusetts Institute of Technology Cambridge, Mass. 02139	(1)
Mr. Glen Rose Grumman Aerospace Air Systems Division/662 Bethpage, Long Island, N.Y. 11714	(1)	Dr. Chauncey Starr Dean of Engineering University of California Los Angeles, California 90009	(1)

Hughes Aircraft Co. Imperial Highway El Segundo, California 90245 Attn: Mr. W. E. Michel (1) Dept. 22-28-00, Bldg. 366 M/S522	Arthur D. Little, Inc. Acorn Park Cambridge, Massachusetts 02140 Attn: Mr. L. Stratton (1)
Philco Ford Corporation 3825 Fabian Way Palo Alto, California 94303 Attn: R. J. Grant, Space Power (1) and Propulsion	North American Rockwell Corporation Los Angeles Division International Airport Los Angeles, California 90009 Attn: Mr. J. Pierro (1)
Sperry Rand Space Support Division 716 Arcadia Huntsville, Alabama 35801 Attn: W. F. Wrye (1)	Dr. Victor Wouk (1) Gulton Industries 212 Durham Avenue Metuchen, New Jersey 08840
Dr. Mahmoud Riaz (1) 1769 Dupont Avenue South Minneapolis, Minnesota 55403	Raytheon Company Sorensen Operation South Norwalk, Connecticut 06854 Attn: Mr. P. Muchnick (1)
Westinghouse Electric Corporation Aerospace Electrical Division Lima, Ohio 45802 Attn: Mr. H. James (1)	Howard B. Hamilton (1) 108 Pennsylvania Hall University of Pittsburgh Pittsburgh, Pennsylvania 15213
Dr. Karl Martinez (1) Boeing Company P. O. Box 3868 Seattle, Washington 98124	Honeywell, Inc. 600 Second Street, North Hopkins, Minnesota 55343 Attn: Mr. J. Lingle (1)
Mosher C. Clifford (1) Edison Electric Institute 3221 Walnut Street Philadelphia, Pennsylvania 19104	Power Information Center (1) University of Pennsylvania 3401 Market Street, Room 2107 Philadelphia, Pennsylvania 19104
Dr. A. H. B. Walker (1) Westinghouse Electric Corporation Research Center Beulah Road Pittsburg, Pennsylvania 15235	Space Technology Laboratories, Inc. One Space Park Redondo Beach, California 90278 Attn: Mr. D. Glaser (1)
Prof. Thomas G. Wilson (1) Duke University School of Electrical Engineering Durham, North Carolina 27707	ITT Research Institute 10 West 35th Street Chicago, Illinois 60616 Attn: Mr. J. Radnick (1)
	Wilmore Electronics Co. (1) P. O. Box 2973 West Durham Station Durham, North Carolina 27705

Lear Siegler, Inc. Power Equipment Division P. O. Box 6719 Cleveland, Ohio 44101 Attn: Mr. R. Dickman	(1)	Mr. Ralph W. Snyder Group Eng. Department 6225 Building 151 1111 Lockheed Way Sunnyvale, California 94088	(1)
Vapor Corporation Vap-Air Division Box 533 Warehouse Point, Connecticut 06088 Attn: Mr. B. E. Butenkoff	(1)	United Airlines, Inc. Engineering Department International Airport San Francisco, California 94128 Attn: Mr. James A. Aldrich	(1)
Prof. R. G. Hoft University of Missouri College of Engineering Columbia, Missouri 65201	(1)	Boeing Aircraft Corporation Commercial Airplane Division P. O. Box 3733 Mail Shop 4199 Seattle, Washington 98124 Attn: Mr. Lewis Weiner	(1)
Bendix Corporation 9 Meriam Street Lexington, Massachusetts 02173 Attn: Mr. Charles E. Rukstuhl	(1)	Lockheed, California Company Building 170 B1 Burbank, California 91503 Attn: Mr. M. J. Cronin	(1)
Westinghouse Electric Corporation Lima, Ohio 45802 Attn: Mr. Dwayne Rife	(1)	American Airlines Maintenance & Engineering Dept. Tulsa, Oklahoma 74151 Attn: Mr. R. C. Munroe	(1)
General Electric Company Wynesboro, Virginia 22980 Attn: Mr. D. L. Plette	(1)	Mr. Robert C. Sprague Sprague Electric Company North Adams, Massachusetts 01890	(1)
Sundstrand Aviation 4747 Harrison Avenue Rockford, Illinois 61108 Attn: Robert C. Baker	(1)	Mr. W. O. Fleckenstein Western Electric Princeton, New Jersey 08540	(1)
General Electric Company Tech. Center Philadelphia, Pennsylvania 19101 Attn: Mr. Archie R. Ruggieri	(1)	Mr. Lionel Boulet Director, Research Institute Quebec Hydroelectric Commission 75 Dorchester, West Montreal, P. Q., Canada	(1)
Bose Corporation 17 Erie Drive Natick, Massachusetts 01760 Attn: Dr. A. Bose	(1)	Dr. S. D. T. Robertson University of Toronto Dept. of Electrical Engineering Toronto, Canada	(1)
Hewlett Packard 620 Page Mill Road Palo Alto, California 94303 Attn: Dr. Richard Soshea	(1)		

Dr. Lester van Atta (1)  
Assistant Dean of Engineering  
University of Massachusetts  
Amherst, Massachusetts 01002

Prof. G. D. Sheckels (1)  
Chairman, Electrical Engineering  
University of Massachusetts  
Amherst, Massachusetts 01002

Dr. M. R. Donaldson (1)  
Chairman, Department of Electrical  
Engineering  
University of South Florida  
Tampa, Florida 33620

Dr. Shirley A. Johnson, Jr. (1)  
Director, Denver Research Institute  
University of Denver  
Denver, Colorado 80210